Software Tools and Guide for Viscoelastic Creep Experiments

Jessica Wehner

A thesis submitted to the faculty of the University of North Carolina at Chapel Hill in partial fulfillment of the requirements for the degree of Master of Science in the Department of Mathematics.

Chapel Hill
2010

Approved by:

M. Gregory Forest

Laura Miller

Shawn Gomez

Abstract

JESSICA WEHNER: Software Tools and Guide for Viscoelastic Creep Experiments. (Under the direction of M. Gregory Forest.)

Models predicting strain as a function of time are fit to data obtained from creep recovery experiments on viscoelastic materials. Here we discuss standard non-inertial and instrument-induced inertial creep experiments. We first summarize and illustrate key signatures, which differentiate the models and highlight properties of creep data. The basic signatures distinguishing a solid versus fluid response, respectively, are: a sudden versus gradual rise when a stress impulse is applied; a sudden versus gradual decline when a constant stress is suddenly removed; and recovery to zero strain versus a finite steady state after the applied stress is removed. For completeness, we discuss development of the models, solution methods, and parameter influence on behavior. Finally, software created by Dr. Ke Xu to estimate the model parameters that best fit the experimental data is adapted to illustrate the influence of experimental noise in parameter recovery.

Table of Contents

List of Figures

Chapter 1

Experimental Rheology

1.1 Overview of Creep Experiments

One tool for exploring the properties of viscoelastic materials is the creep experiment. Typically, a shear stress (force per unit area, given here as τ) is imposed on the material in a prescribed manner (with a known magnitude usually measured in pascals and with dictated on and off times) by a rheometer. The sample is trapped between two small plates in the rheometer, and shear stress is applied to the fluid through the controlled torque rotation of the top plate relative to the bottom. The top and bottom plate can both be flat and parallel, as in a parallel plate rheometer; or the top plate can be an inverted cone with a very shallow angle, as in the cone and plate rheometer. A controlled torque is imparted to the top plate, and its angular deflection is measured with high accuracy as it rotates with influence from the thin layer of material beneath it. From this we can take measurements of how the sample deforms under the applied stress and how it recovers once the imposed stress is removed.

The geometry of a cone and plate rheometer is depicted below in Figure 1.1. The values R and β are known, where R is the length from the center of the plate to the edge, and β is the angle the cone makes with the bottom plate, usually about 1°. The angular deflection ϕ is recorded during the experiment. With these values, shear strain (denoted here as γ and unitless) can be calculated by $\gamma = \frac{\phi}{\beta}$, or the ratio of the displacement to the thickness of the sample. See

(Macosko94) for further details.

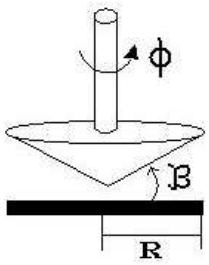

Figure 1.1: Geometry of a cone and plate rheometer with diameter R, cone angle β and angular deflection ϕ.

Under constant stress as in these experiments, the linear response of a viscoelastic material is proportional to the imposed stress. (This will be evident below when we give the model equations and their closed-form solutions.) Thus, it is natural to normalize strain by the imposed stress. This defines the compliance, $J = \gamma/\tau$. In this manner, the material response J is independent of the value of the input stress. A good experimental test of linear response is to run the experiment at several stress levels. All the data should collapse onto a single curve, the compliance curve. The mathematical models used here, which predict strain values, are converted to compliance before use with compliance data.

By plotting the compliance as a function of time, we can obtain graphs with standard features which are unique for different types of materials. An overarching goal is to find mathematical models which best reflect these features, to which end there are many standard mechanical models used in practice which will be discussed in this document. Additionally, two types of creep experiments can be performed and each may collect unique information. These are the inertial and non-inertial experiments.

Performing an inertial experiment means that the inertia of the rotating parts of the rheometer is allowed to enhance the elasticity of the material resulting in oscillatory behavior in the response, sometimes referred to as 'ringing'. Initially, only non-inertial experiments were performed, in which the inertia within the machine was damped to a high degree to avoid in-

terference with the data. However, a very small amount of oscillatory behavior present at the beginning of these experiments could be noted. These first few moments would be removed from the data to prevent it from interfering with further analysis. It was then discovered, as noted in (Barav98), that the inertia of the instrument could be coupled to the material's elasticity to aid in the study of thixotropy. Thixotropy can be described as the time dependent change in viscosity that a material might undergo during a stress experiment. Although we are not concerned with how to model thixotropy in this thesis, we will provide evidence while fitting to experimental data that thixotropy occurs in certain materials. It is important to consider the coupling of instrumental inertia for other reasons than to study thixotropy; these include a much shorter timescale on which useful information may be collected and the ability to infer more information from a single experiment.

Material behavior

For a simple elastic response, the governing equation is Hooke's law: stress (τ) is proportional to strain (γ) with the shear modulus (G) as the constant of proportionality, $\tau = G\gamma$. The simplest equation to describe a purely viscous response is Stokes relation: stress (τ) is proportional to rate of strain ($\dot{\gamma}$) with constant of proportionality the viscosity (η), $\tau = \eta\dot{\gamma}$. Both of these models have been around since the 1660s. Let's observe how these simple equations respond to an imposed constant stress that is turned on at t_0 and turned off at t_1 (this is equivalent to a top hat function which can be written as $\tau = H(t-t_0) - H(t-t_1)$).

Hooke's law can be solved directly for γ, $\gamma = \frac{\tau}{G}$. Thus, the strain of a pure solid will mimic the top hat function but with a changed magnitude dependent on G. At the onset of stress, the solid will suddenly reach some constant strain, maintain that strain for the duration of the applied stress, and then suddenly recover to its resting configuration (recover fully to 0 strain). This is a result of a solid's ability to store stress as it is applied and release it once stress is removed. As another example, if the stress is sinusoidal instead of top hat, the response of an

elastic material will remain in phase with the stress. Just consider $\tau = \sin(t)$ and observe that $\gamma = \frac{1}{G}\sin(t)$ has a new amplitude but remains in phase.

Solving Stoke's Law for γ requires an integration of the applied stress; in this case, the integration of two step functions results in two linear functions. The result is $\gamma = \frac{1}{\eta}[(t-t_0)H(t-t_) - (t-t_1)H(t-t_1)]$. This and the elastic response above are depicted in Figure 1.2. At the onset of stress, the pure liquid will strain linearly. Once the stress is removed, the liquid will maintain the acquired configuration and will not recover any strain. This is because a purely viscous material cannot store stress and hence deforms continuously as shear stress is applied. The strain of a fluid will be $\pi/2$ radians out of phase with a stress that is applied sinusoidally. For example, if $\tau = \sin(t)$, then γ will be given by a cosine function, which is $\pi/2$ radians out of phase with sine.

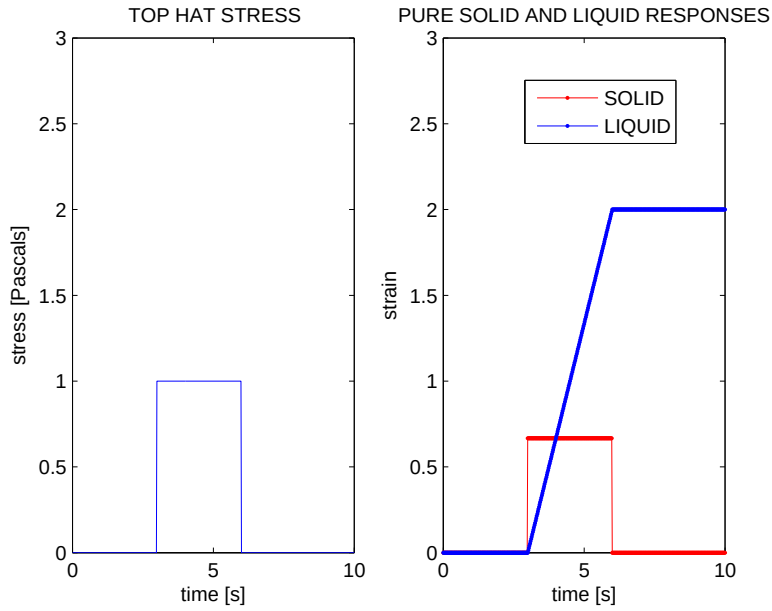

Figure 1.2: The response of a pure solid (red) and a pure liquid (blue) to an applied top hat stress.

Viscoelastic materials exhibit both viscous and elastic properties, yet can be more solid-like or liquid-like in their response to constant or phasic shear stress. Thus, an initial focus of creep experiments is to identify whether a viscoelastic material is more fluid-like or solid-

like at the applied stress level. A further complicating observation is that many viscoelastic materials are solid-like at sufficiently low stress levels, yet liquid-like above a stress threshold. This thesis will only give an example of such materials, but the tools presented here can detect such behavior simply by varying stress levels in a series of creep experiments across the critical threshold.

It should be noted that the most general distinction of 'liquid-like' or 'solid-like' used to categorize the models in Chapter 2 is chosen here based on end behavior - if the model recovers to 0 strain after stress is turned off, it is denoted as a linear viscoelastic solid; if the model recovers to some positive steady state strain when stress is turned off, it is denoted as a linear viscoelastic liquid. The other features considered here, such as an initial jump in strain at the onset of an applied stress or a sudden drop in strain once stress is removed, can also be considered liquid-like or solid like. However, because of our choice to use end behavior as the broadest category, the other features will be intermixed between solid- and liquid-like models.

1.2 Mechanical Models

The basic viscous and elastic elements can be represented as mechanical forms having a governing constitutive law. The basic viscous element is represented as a dashpot. As its purpose is to represent a purely viscous response, it is governed by Stokes relation described above: $\tau = \eta\dot{\gamma}$. The basic elastic element, meant to represent a purely elastic response, is represented as a spring and is governed by Hooke's law: $\tau = G\gamma$. See Figures 1.3 and 1.4.

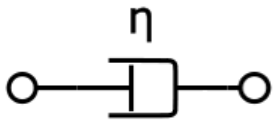

Figure 1.3: The viscous element represented as a dashpot, with viscosity η.

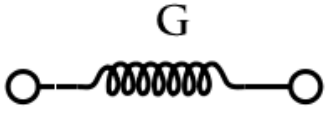

Figure 1.4: The elastic element represented as a spring with shear modulus G.

To build a viscoelastic material, the spring and dashpot elements can be combined in series and parallel configurations, achieving new behavior with at least two parameters - G and η. Certain rules define how the governing equations are combined. These configurations and their equations have given rise to the several standard linear viscoelastic models used today and are presented in detail in further sections of this document. However, to give a thorough example of how one such model might be developed, we shall now go through the steps which lead to the standard Three Parameter Maxwell model. All other models are developed in the same manner; an excellent reference for all of these models is (Tschoegl89).

Deriving the Three Parameter Maxwell model

The Three Parameter Maxwell mechanical model is created by combining a Maxwell element in parallel with a spring. Thus, first we must know how to create the Maxwell element. The Maxwell element is the series combination of one spring and one dashpot, as shown below. The rule for series configurations is that the strains add and the stresses are distributed equally.

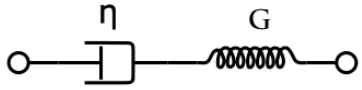

Figure 1.5: Two Parameter Maxwell element

For the dashpot (viscous element) we have $\tau_v = \eta\dot{\gamma}_v$. For the spring (elastic element) we have $\tau_e = G\gamma_e$. Adding strains means that the overall strain of the two parameter model is the sum of the strains of each element, $\gamma = \gamma_e + \gamma_v$. Thus,

$$\begin{aligned} \dot{\gamma} &= \dot{\gamma}_e + \dot{\gamma}_v \\ &= \frac{\dot{\tau}_e}{G} + \frac{\tau_v}{\eta} \end{aligned} \tag{1.1}$$

Since equating stresses means that $\tau = \tau_e = \tau_v$, we can substitute τ, the overall stress of the two parameter model, for τ_e and τ_v, the stresses of the individual elastic and viscous elements, respectively. Thus, we have $\dot{\gamma} = \frac{\dot{\tau}}{G} + \frac{\tau}{\eta}$. We can divide through by η to get as the constitutive law of the two parameter Maxwell element the equation $\eta\dot{\gamma} = \frac{\eta}{G}\dot{\tau} + \tau$, which we note is trivial to solve for γ/τ_0 by one integration.

To create the Three Parameter Maxwell model we combine the Maxwell element in parallel with a spring, as shown below. Now, the law which governs the maxwell element was found

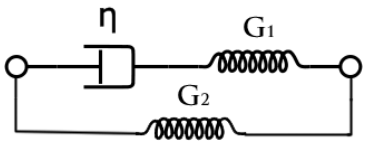

Figure 1.6: Three Parameter Maxwell element

to be $\eta_1\dot{\gamma}_1 = \frac{\eta_1}{G_1}\dot{\tau}_1 + \tau_1$, and the law which governs the spring is given by $\tau_2 = G_2\gamma_2$ (using subscripts to differentiate between parameters). We wish to combine these two elements (the spring and the maxwell) in parallel, for which the rule is to add stresses and distribute strains equally. Thus, noting that $\dot{\tau}_1 = \dot{\tau} - \dot{\tau}_2 = \dot{\tau} - G_2\dot{\gamma}$, we have

$$\begin{aligned} \tau &= \tau_1 + \tau_2 \\ &= \left(\eta_1\dot{\gamma}_1 - \frac{\eta_1}{G_1}\dot{\tau}_1\right) + G_2\gamma_2 \\ &= \eta_1\dot{\gamma} - \frac{\eta_1}{G_1}\dot{\tau}_1 + G_2\gamma \\ &= \eta_1\dot{\gamma} - \frac{\eta_1}{G_1}(\dot{\tau} - G_2\dot{\gamma}) + G_2\gamma \end{aligned} \tag{1.2}$$

From here we can simplify, obtaining

$$\dot{\tau} + \frac{G_1}{\eta_1}\tau = (G_1 + G_2)\dot{\gamma} + \frac{G_1}{\eta_1}G_2\gamma \tag{1.3}$$

as the constitutive law for the Three Parameter Maxwell model.

1.3 Illustration of Experimental Data

The data used here are the same as in (Xu2009), for which she describes the preparation as follows:

> ... low melting point agarose (Sigma product number A9414) is mixed to 0.3% in the same buffer (0.2M NaCl, 0.01EDTA, and 0.01% Sodium Azide). The samples' rheological properties are determined by a Bohlin Gemini Rheometer in both cone and plate (60mm diameter, 1 degree, 7.9103mm3 in volume) and parallel plate (20mm diameter, 50um gap, 63mm3 in volume) geometries under the stress amplitude sweep mode.

In order to illustrate the models, exact data generated directly from each model will be used. However, in reality experimental data is not always 'clean' and therefore cannot be expected to match perfectly any one model. For example, creep experiments are best done at low stress levels. With too high stress (above the stress threshold), the results are compromised and informative features cannot be extracted. Consider Figure 1.7 showing agarose data at a stress of 2 pascals. The compliance has no curvature - it essentially ramps up continuously until the stress is removed at 10 seconds, at which point it relaxes to a high value and remains there, similar to a pure liquid. The stress was high enough to 'overpower' the elasticity in the sample, and any stress at this level or higher will be unable to capture the viscoelastic properties of the material.

Experimental error is also always present in the data. Generally it is easy to see what the features of the graph are despite the error. Because it is random error we are capable of ignoring unusually extreme values and inferring what the curve 'should' look like. The data in Figure 1.8 looks like it could be very noisy data. In actuality, most of the 'noise' is rather high frequency oscillations that are not apparent under this scaling. However, in the later parts of the graph the oscillations do not appear to be dying off as expected, and this could be a result of a

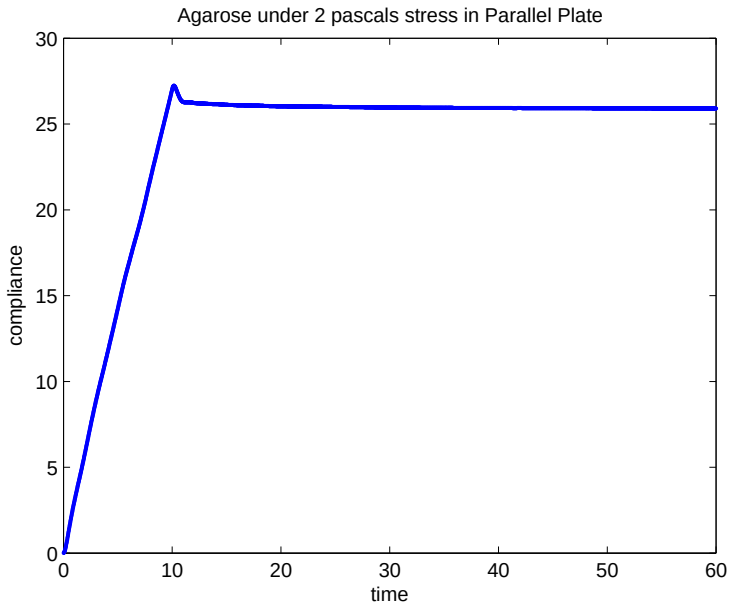

Figure 1.7: When experiments are performed on agarose under too high of a stress, the stress threshold is passed and the material resembles a pure liquid rather than a viscoelastic fluid.

small amount of noise present while viewing a small range. (i.e., if the data were plotted with a larger range, the experimental error would be relatively smaller and the data would appear less noisy.) One should also keep in mind that experimental data is discrete. In the data considered here, time steps of .02 seconds are used. If the frequency of inertial data is higher than the sampling frequency, then we will be unable to detect oscillations and the data could instead just appear noisy.

A note on parameter values

The properties of purely viscous and elastic materials are consistent regardless of the type of stress imposed on them. On the contrary, viscoelastic materials would be expected to behave much differently depending on the way they are being stressed, say for a sinusoidal stress of low versus high frequency. It is for this reason that different types of experiments are important and necessary for probing many different realms of linear viscoelastic responses. It is also

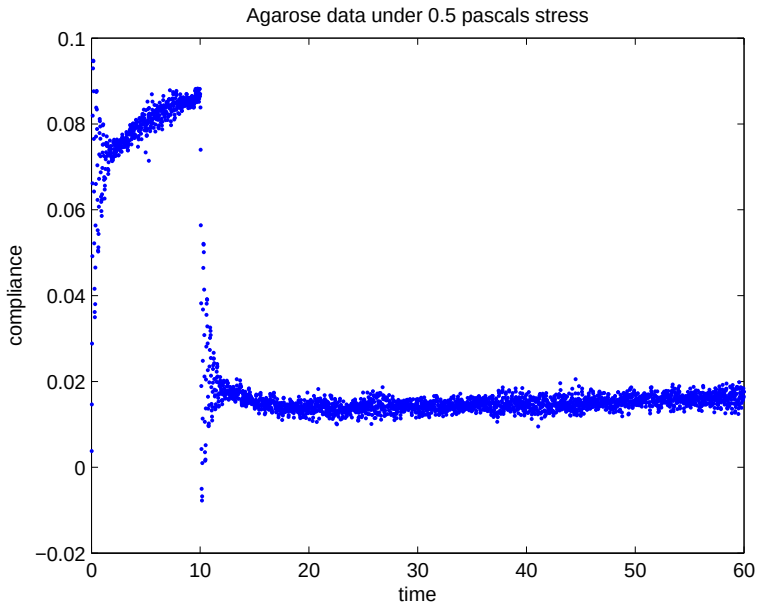

Figure 1.8: Highly oscillatory agarose data appears noisy.

because of this that it is impossible to identify single parameter values which best describe any given viscoelastic material. At best, a range of values must be given to describe a range of driving forces. These ranges can be quite large. Experimentally, the added difficulty is that the prepared samples cannot be perfectly the same, resulting in a range of recorded experimental parameters.

Regardless of the fact that the true state of the material varies greatly, our methods for extracting parameter guesses can also fluctuate. In the context discussed here, statistical regression is performed on sample data to determine the best fit parameters. Should this regression be performed on the entire data set, or on smaller pieces of the data? If so, how small, and which pieces? It is important to decide ahead of time, because parameters inferred from different sections of the same data can report largely different numbers (evidence of nonlinear behavior, examined further in Chapter 4). As an example, consider this summary of results obtained by making multiple fits on two data sets. One data set is from an inertial creep experiment on 0.3% agarose at a 0.5 Pascal stress level. The second is from an inertial creep experiment on

0.2% agarose at a 0.5 Pascal stress level. The Inertial Maxwell-Jeffrey and Inertial Kelvin-Voigt models were fit to these data sets at time intervals $[0,1]$, $[0,4]$ and $[0,10]$. From the table below we can see that η_1 seems to have the largest range, in one case ranging from 59 to 464, while the parameter G remains very consistent across each model on the same data set. More will be discussed on the sensitivity of parameters in Chapter 4.

0.3% Agarose

Fit for Inertial Maxwell-Jeffrey

	η_1	G	η_2	α
$[0,1]$	59.43	17.978	0.163	0.044
$[0,4]$	230.11	15.795	0.176	0.038
$[0,10]$	463.16	14.731	0.183	0.036

Fit for Inertial Kelvin-Voigt

	η	G	α
$[0,1]$	0.194	15.616	0.038
$[0,4]$	0.191	13.879	0.033
$[0,10]$	0.206	12.703	0.030

0.2% Agarose

Fit for Inertial Maxwell-Jeffrey

	η_1	G	η_2	α
$[0,1]$	7.297	2.526	0.074	0.048
$[0,4]$	37.290	2.152	0.095	0.041
$[0,10]$	103.779	2.001	0.100	0.038

Fit for Inertial Kelvin-Voigt

	η	G	α
$[0,1]$	0.124	2.135	0.042
$[0,4]$	0.104	1.923	0.036
$[0,10]$	0.109	1.823	0.034

Chapter 2

Non-Inertial Models

2.1 Overview of Non-Inertial Models

In a creep experiment without inertia, stress is applied to the material by a rheometer. A constant applied stress can be turned on and left on (step stress), turned off after an interval of time (top hat stress), or applied as a train of pulses. Only step and top hat stress experiments are considered in this thesis. The material responds to the stress by deforming, and the resulting displacement is measured and converted to strain (or compliance), which is plotted against time to produce a strain response curve. The inertia of the instrument is able to be damped to a high degree to keep from interfering with the strain measurements.

Different characteristics in the responses can then potentially be captured by one of several standard models: the Two Parameter Maxwell, Three Parameter Maxwell, Two Parameter Kelvin-Voigt, Three Parameter Kelvin-Voigt or the Maxwell-Jeffrey. Each is a mechanical model corresponding to a linear differential constitutive law. The continued usage of these models has historical precedence coming from the convenience of their ability to be solved in closed form and their ability to capture key creep features of simple viscoelastic liquids and solids (whose distinction we emphasize below). In Section 2.3, each model is categorized as a linear viscoelastic liquid or solid model and is given along with its constitutive law. Solutions in a creep experiment are given under a top hat stress, where the stress is turned on at time t_0

and turned off at time t_1. The imposed form of stress used for obtaining the given solutions is $\tau(t) = \tau_0 (H(t-t_0) - H(t-t_1))$, where

$$H(t-x) = \begin{cases} 0 & \text{if } t < x; \\ 1 & \text{if } t \geq x; \end{cases}$$

is the step function. (Solutions for step stress are found by ignoring the terms containing $t - t_1$, or equivalently, taking t_1 to infinity.) For $t_0 = 0$, $t_1 = 10$ and $\tau_0 = 1$, the τ top hat function will look like the graph in Figure 2.1. These are the same on and off times for the applied stress used in all the experiments considered in this thesis.

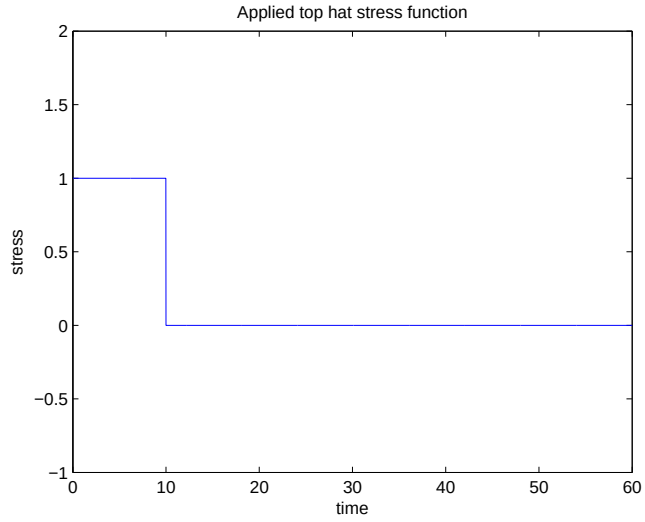

Figure 2.1: Graph of an applied top hat stress.

As noted in Section 1.3, the properties of viscoelastic materials depend on the way they are being stressed. This top hat form of applied stress is equivalent to a sinusoidal stress function with zero frequency. Thus, the material properties that are inferred are only useful for describing the material at a very low frequency.

Graphical illustrations of each model's solution are presented showing typical behavior of the model. Recall that the most general distinction of 'liquid-like' or 'solid-like' used to

categorize the models here is made based on end behavior rather than some other type of feature. Before presenting all of the models and their solutions, the next section illustrates the Laplace Transform method for solving the Three Parameter Maxwell constitutive law (a differential equation) under a step stress.

2.2 Example: Derivation of Analytical Solution to Three Parameter Maxwell Model

We have seen in Section 1.2 how the constitutive law for the Three Parameter Maxwell mechanical model is derived. It is given by

$$\dot{\tau} + \frac{G_1}{\eta_1}\tau = (G_1 + G_2)\dot{\gamma} + \frac{G_1}{\eta_1}G_2\gamma \tag{2.1}$$

In creep experimentation, we impose a known stress. As a simple example, let us use the stress function $\tau(t) = H(t - t_0)$, the step function which is zero for $t < t_0$ and is one elsewhere. This is equivalent to a constant stress of one Pascal suddenly turning on at time t_0. A top hat stress function (in which the stress is suddenly turned off at time t_1), would essentially be solved twice - once for $H(t - t_0)$ and once for $H(t - t_1)$ - but the method is exactly the same.

Knowing $\tau(t)$, Equation (2.1) is a first order differential equation for $\gamma(t)$. Using the Laplace Transform is a simple way to solve this equation for $\gamma(t)$: we first take the transform of the equation (inputting the transform of the stress function), then we solve the resulting equation for $\Gamma(s)$ in transform space, and finally we invert the equation back to real space.

To simplify the constitutive law, we first let $\lambda_1 = \frac{\eta_1}{G_1}$. This gives us

$$\dot{\tau} + \frac{1}{\lambda_1}\tau = (G_1 + G_2)\dot{\gamma} + \frac{G_2}{\lambda_1}\gamma \tag{2.2}$$

Taking the Laplace Transform of each side of (2.2) we obtain

$$\left(s+\frac{1}{\lambda_1}\right)T(s)=\left((G_1+G_2)s+\frac{G_2}{\lambda_1}\right)\Gamma(s) \tag{2.3}$$

We wish to impose $\tau(t)=H(t-t_0)$, which in transform space is equivalent to $T(s)=\frac{1}{s}e^{-t_0 s}$. Inputting this to (2.3) and solving for $\Gamma(s)$ we have

$$\begin{aligned}\Gamma(s) &= \frac{s+\frac{1}{\lambda_1}}{(G_1+G_2)s+\frac{G_2}{\lambda_1}}\frac{1}{s}e^{-t_0 s}\\ &= \frac{1}{G_1+G_2}\left[\frac{1}{s+\frac{G_2}{(G_1+G_2)\lambda_1}}+\frac{\frac{1}{\lambda_1}}{s\left(s+\frac{G_2}{(G_1+G_2)\lambda_1}\right)}\right]e^{-t_0 s}\end{aligned} \tag{2.4}$$

In order to invert the transform, we must break up the $\frac{\frac{1}{\lambda_1}}{s\left(s+\frac{G_2}{(G_1+G_2)\lambda_1}\right)}$ term into simplified terms that we know how to invert. We can do this using partial fractions. Observe,

$$\frac{1}{s\left(s+\frac{G_2}{(G_1+G_2)\lambda_1}\right)}=\frac{A}{s}+\frac{B}{s+\frac{G_2}{(G_1+G_2)\lambda_1}} \implies 1=A\left(s+\frac{G_2}{(G_1+G_2)\lambda_1}\right)+B(s) \tag{2.5}$$

With appropriate choices for s (try $s=0$ and $s=\frac{-G_2}{(G_1+G_2)\lambda_1}$), we can solve for the coefficients A and B to be $A=\frac{(G_1+G_2)\lambda_1}{G_2}$ and $B=\frac{-(G_1+G_2)\lambda_1}{G_2}$. Now Equation (2.4) becomes

$$\begin{aligned}\Gamma(s) &= \frac{1}{G_1+G_2}\left[\frac{1}{s+\frac{G_2}{(G_1+G_2)\lambda_1}}+\frac{G_1+G_2}{G_2 s}-\frac{G_1+G_2}{G_2\left(s+\frac{G_2}{(G_1+G_2)\lambda_1}\right)}\right]e^{-t_0 s}\\ &= \frac{1}{G_1+G_2}\left[\left(\frac{G_1+G_2}{G_2}\right)\frac{1}{s}+\left(1-\frac{G_1+G_2}{G_2}\right)\left(\frac{1}{s+\frac{G_2}{(G_1+G_2)\lambda_1}}\right)\right]e^{-t_0 s}\\ &= \frac{1}{G_1+G_2}\left[\left(\frac{G_1+G_2}{G_2}\right)\frac{1}{s}-\frac{G_1}{G_2}\left(\frac{1}{s+\frac{G_2}{(G_1+G_2)\lambda_1}}\right)\right]e^{-t_0 s}\end{aligned} \tag{2.6}$$

Next we wish to take the inverse Laplace Transform of (2.6). We will use the following three properties: $L^{-1}(\frac{1}{s}) = H(t), L^{-1}(F(s+a)) = f(t)e^{-at}$, and $L^{-1}(F(s)e^{-as}) = f(t-a)$. Applying these to (2.6) and letting $\lambda = \frac{G_2}{(G_1+G_2)\lambda_1}$, the solution to the Three Parameter Maxwell model under a step stress can be written as

$$L^{-1}(\Gamma(s)) = \gamma(t) = \frac{1}{G_1+G_2}\left[H(t-t_0)\left(\frac{G_1+G_2}{G_2} - \frac{G_1}{G_2}e^{-(t-t_0)/\lambda}\right)\right] \tag{2.7}$$

2.3 Linear Viscoelastic Liquid Models

Liquid-like materials cannot store stress, rather they dissipate stress - this is reflected in a response curve that never recoils to zero strain (that is, never regains its original conformation) after the imposed stress is removed. Indeed a pure liquid does not recover any stress-induced strain. The Two Parameter Maxwell Model and the Maxwell-Jeffrey Model are candidates for modeling fluid-like materials, or viscoelastic liquids. It should be emphasized that while the Two Parameter Maxwell model satisfies the basic properties of a fluid model, it is overly simplistic when solved in creep and is not appropriate for modeling a linear viscoelastic material. It is included here for completeness.

The measured strain in each model increases steadily under constant stress and relaxes to a constant positive value after stress is removed, as seen in Figure 2.2 below. This behavior comes from the free dashpot element present in series in each mechanical model. (Recall that the dashpot is the viscous element.) Its presence leads to a factor of $(t-t_0)$ in the final step stress solution, which causes the end behavior to go to infinity as t increases. A factor of $(t-t_0)-(t-t_1)$ appears in the final top hat stress solution. In this case, the two large terms cancel as t goes to infinity, and the remaining terms are constant. Distinguishing the two terms (besides the fact that the Two Parameter Maxwell model is completely linear, while the Maxwell-Jeffrey model has curvature) is the sudden jump at the onset and offset of stress in the Two Parameter Maxwell model.

The Two Parameter Maxwell Model

Mechanical Model

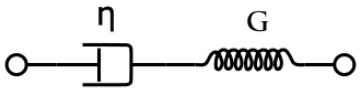

Constitutive Law $\lambda\dot{\tau}+\tau=\eta\dot{\gamma}$, where $\lambda=\eta/G$

Solution in Creep

$$\gamma(t)=\frac{\lambda\tau_0}{\eta}\left[H(t-t_0)-H(t-t_1)\right]+\frac{\tau_0}{\eta}\left[(t-t_0)H(t-t_0)-(t-t_1)H(t-t_1)\right]$$

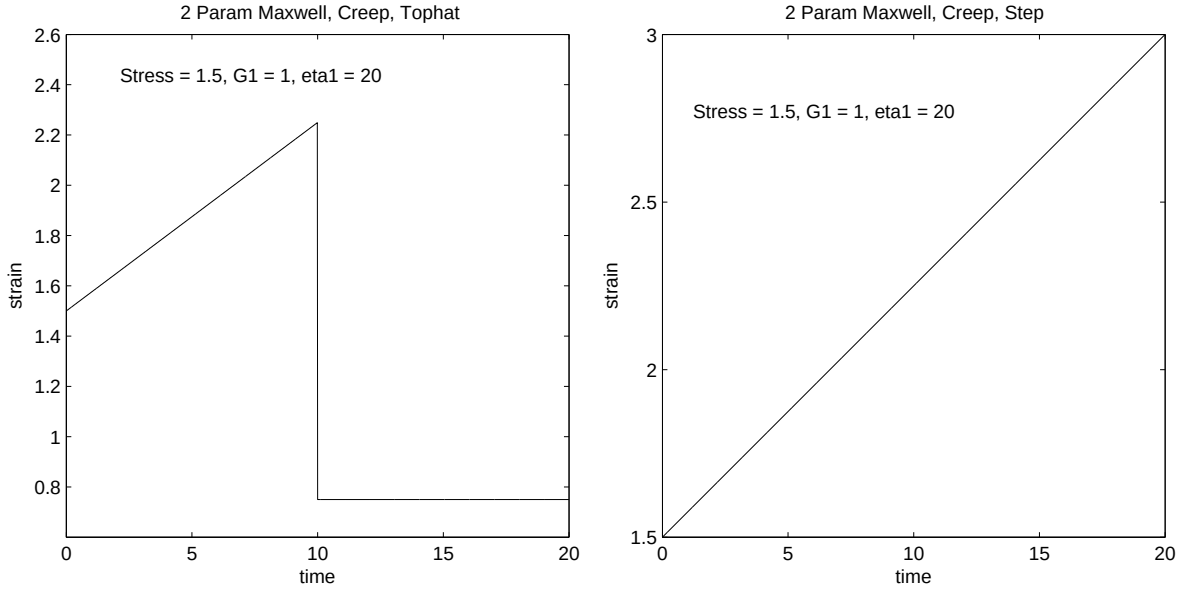

Figure 2.2: The Two Parameter Maxwell Model under a top hat (left) and step (right) stress.

The Maxwell-Jeffrey Model

Mechanical Model

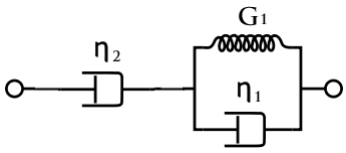

Constitutive Law $(\eta_1+\eta_2)\dot{\tau}+G\tau=\eta_2 G\dot{\gamma}+\eta_1\eta_2\ddot{\gamma}$

Solution in Creep

$$\begin{aligned}\gamma(t) &= \frac{\tau_0}{G}\left[H(t-t_0)-H(t-t_1)\right]+\frac{\tau_0}{\eta_2}\left[(t-t_0)H(t-t_0)-(t-t_1)H(t-t_1)\right]\\ &\quad -\frac{\tau_0}{G}\left[H(t-t_0)e^{-\frac{(t-t_0)G}{\eta_1}}-H(t-t_1)e^{-\frac{(t-t_1)G}{\eta_1}}\right]\end{aligned}$$

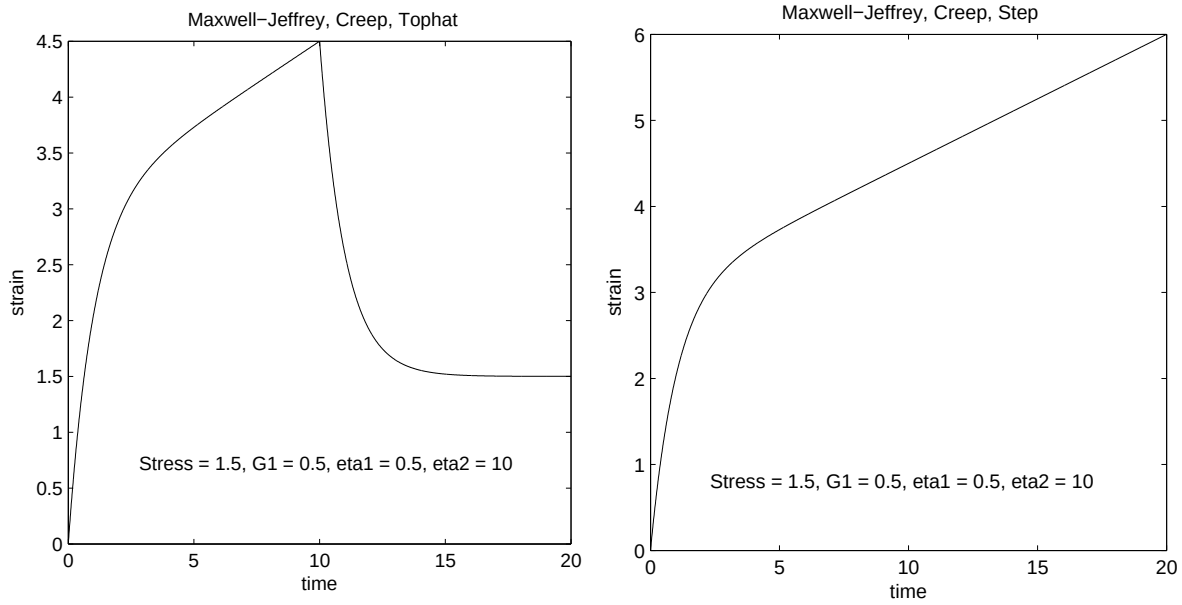

Figure 2.3: The Maxwell-Jeffrey Model under a top hat (left) and step (right) stress.

2.4 Linear Viscoelastic Solid Models

Solid-like materials are distinguished by their ability to store stress. This is reflected in a response curve that recovers to zero strain when stress is removed - the stored stress pulls the material back to its original shape. This behavior comes from the free spring element present in parallel in each mechanical model. (Recall that the spring is the storage element.) However, it is the absence of the free dashpot - which leads to the absence of factors of t - which contributes to the long time recovery to zero behavior. Only step function and negative exponential terms appear in the solutions. For large t, the negative exponential terms all approach 0. In step stress, a single step function is left, causing the end behavior to asymptotically approach a positive constant value. In top hat stress, the difference of two step functions remain (each having the same magnitude), and so after long enough time, their difference approaches 0.

The 3 Parameter Maxwell or 3 Parameter Voigt models are good candidates for modeling solid-like materials and are known as the linear viscoelastic solid models. Each fully recovers to zero strain under a finite duration top hat stress, and each levels out to a steady state strain under a constant applied stress. Each also has an initial jump in strain at the onset of an applied stress and another jump at the offset of stress - another solid-like quality. The 2 Parameter Voigt model is also categorized here for having similar end behavior. However, this model behaves more like a fluid in that the initial strain begins at 0 and gradually rises (there is no sudden jump). This may be good for modeling viscoelastic materials that have borderline viscous and elastic properties.

The Three Parameter Maxwell Model

Mechanical Model

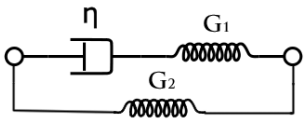

Constitutive Law $\dot{\tau} + \frac{1}{\lambda_1}\tau = (G_1 + G_2)\dot{\gamma} + \frac{G_2}{\lambda_1}\gamma$, where $\lambda_1 = \eta/G_1$

Solution in Creep

$$\gamma(t) = \frac{\tau_0}{G_1 + G_2}\left[H(t-t_0)\left(\frac{G_1+G_2}{G_2} - \frac{G_1}{G_2}e^{-\frac{t-t_0}{\lambda_1}}\right) - H(t-t_1)\left(\frac{G_1+G_2}{G_2} - \frac{G_1}{G_2}e^{-\frac{t-t_1}{\lambda_1}}\right)\right]$$

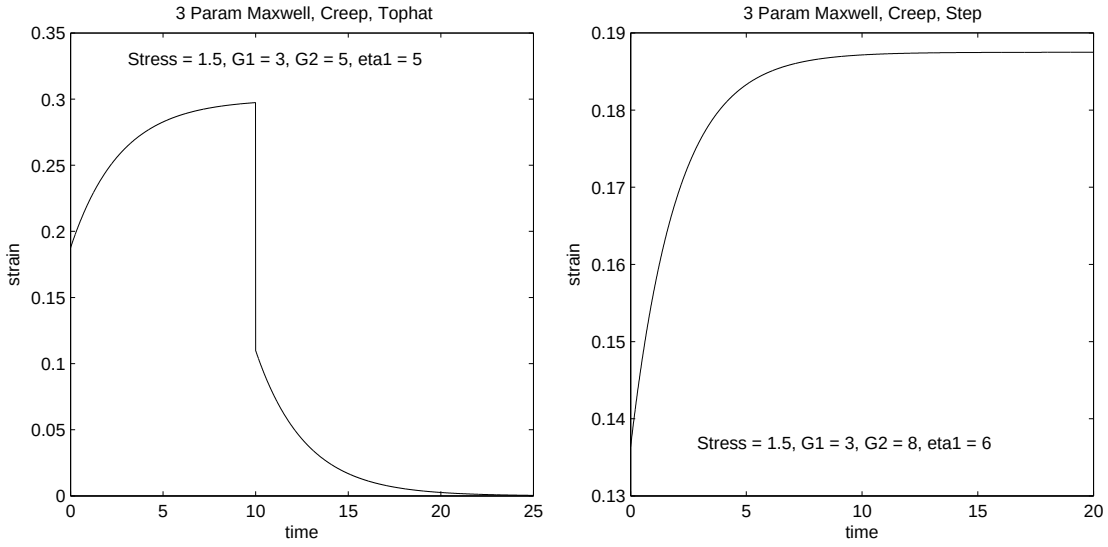

Figure 2.4: The Three Parameter Maxwell Model under a top hat (left) and step (right) stress.

The Two Parameter Kelvin-Voigt Model

Mechanical Model

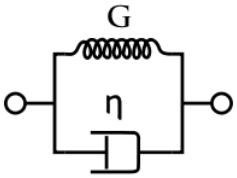

Constitutive Law $\tau = G\gamma + \eta\dot{\gamma}$

Solution in Creep

$$\gamma(t) = \frac{\tau_0}{G}\left[H(t-t_0)\left(1-e^{-\frac{t-t_0}{\lambda}}\right) - H(t-t_1)\left(1-e^{-\frac{t-t_1}{\lambda}}\right)\right], \text{ where } \lambda = \eta/G$$

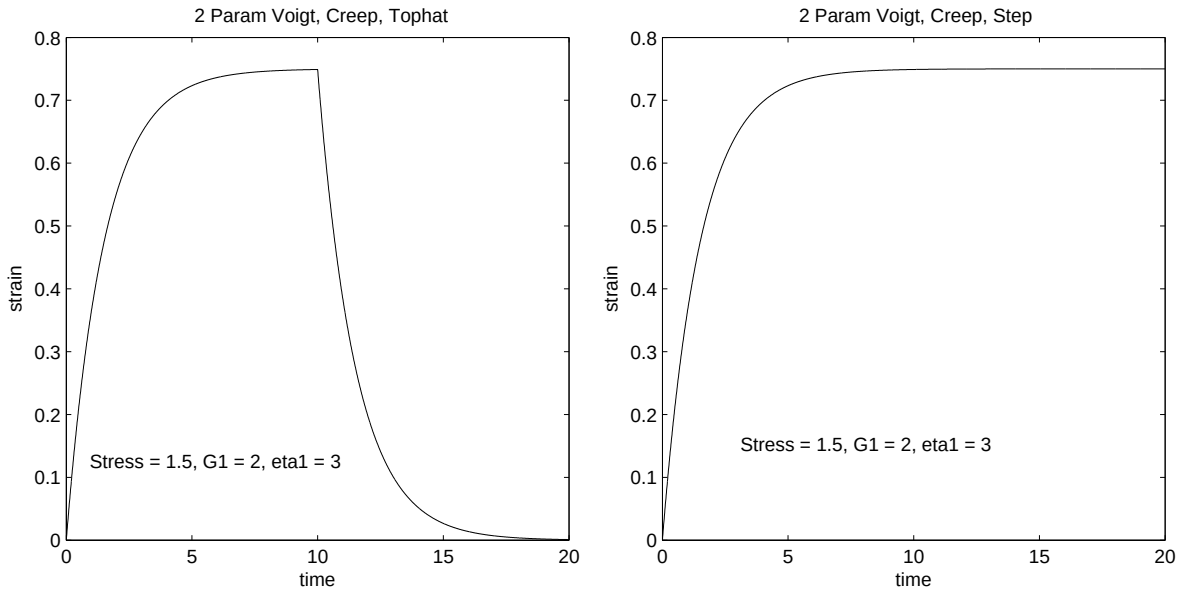

Figure 2.5: The Two Parameter Kelvin-Voigt Model under a top hat (left) and step (right) stress.

The Three Parameter Kelvin-Voigt Model

Mechanical Model

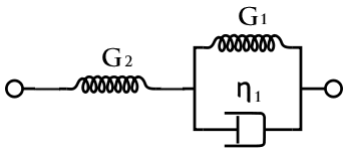

Constitutive Law $\frac{\eta_1}{G_1}\dot{\gamma}+\gamma=\frac{\eta_1}{G_1G_2}\dot{\tau}+(\frac{1}{G_1}+\frac{1}{G_2})\tau$

Solution in Creep

$$\gamma(t) = \frac{\tau_0}{G_2}H(t-t_0)\left[\frac{G_1+G_2}{G_1}-\frac{G_2}{G_1}e^{-\frac{t-t_0}{\lambda_1}}\right]-\frac{\tau_0}{G_2}H(t-t_1)\left[\frac{G_1+G_2}{G_1}-\frac{G_2}{G_1}e^{-\frac{t-t_1}{\lambda_1}}\right]$$

where $\lambda_1=\eta_1/G_1$

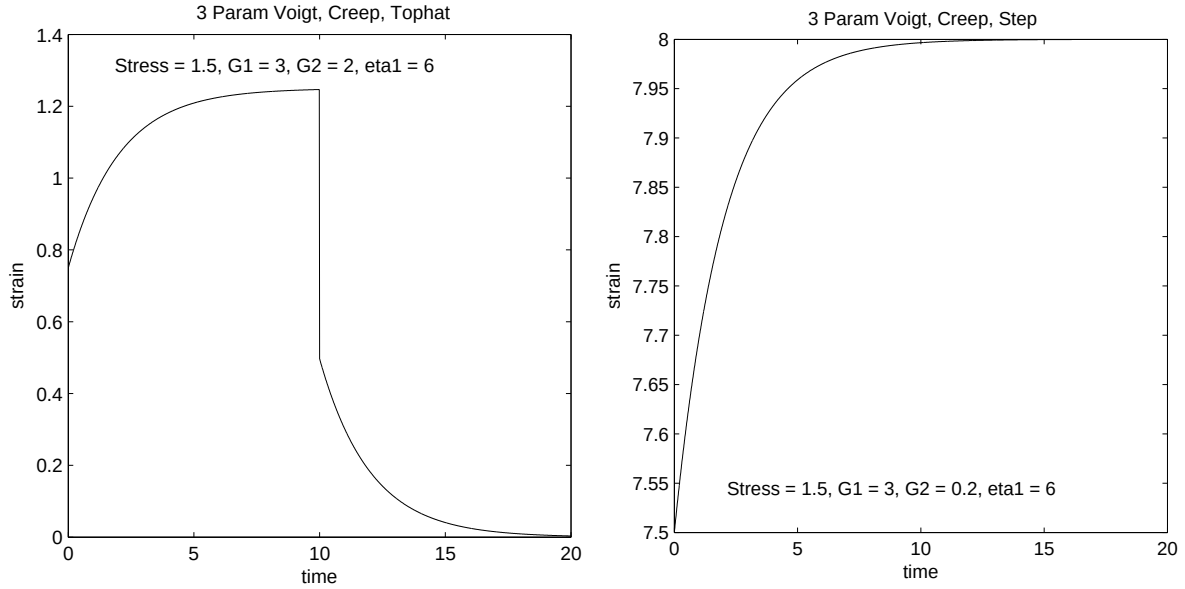

Figure 2.6: The Three Parameter Kelvin-Voigt Model under a top hat (left) and step (right) stress.

2.5 Summary of Model Signatures of Non-Inertial Creep Experiments

Follow this guide for creep experiments done under a step or top hat stress to help choose the best model to fit to your data. Refer to the figures above for examples of each model, and refer to Section 4.2 for demonstrations of how each is used to fit experimental data.

1. Look at the terminal behavior of the strain response curve for your material. In top hat stress, does it approach a positive finite steady state rather than recovering to zero? In step stress, does it maintain positive slope rather than leveling off?

   (a) If yes to either, the material exhibits fluid-like tendencies. Although the Two Parameter Maxwell model falls in this category, we do not recommend it. Refer instead to the Maxwell-Jeffrey model and see #2.

   (b) If the curve recovers to zero in top hat stress, or if it levels off in step stress, this is a solid-like quality. The Two Parameter Voigt, Three Parameter Voigt, or Three Parameter Maxwell model will capture this feature. See #3.

2. In either step or top hat stress, is there a sudden jump at time 0?

   (a) If so, the Maxwell-Jeffrey model will not capture this jump, which is a solid-like feature. If it is a significant factor in the data, you may need to refer to a solid-like model (see #3) or a model not discussed in this thesis (perhaps a 4 parameter or nonlinear model).

   (b) If the initial value is 0, try the **Maxwell-Jeffrey** model first, which also exhibits a gradual decline upon the removal of stress.

3. Does the strain response curve have a sudden jump at time 0 in either top hat or step stress?

(a) If so, the **Three Parameter Maxwell** and **Three Parameter Voigt** models can both capture this feature, which is also a solid-like feature. These two models are essentially the same, and in addition they exhibit a sudden drop upon the removal of stress.

(b) If instead the curve begins close to zero, try the **Two Parameter Voigt** model. This model is fluid-like in the way the strain gradually rises from 0, and solid-like in the way it recovers to 0 upon the removal of stress.

Chapter 3

Inertial Models

3.1 Overview of Inertial Models

In creep experiments that utilize instrumental inertia, a Rheometer imparts a controlled stress on the material, and the undamped inertia of the instrument is allowed to enhance the elasticity of the material, causing ringing behavior to occur. The rheometer measures angular displacement as the material is allowed to relax and converts this to a measurement of compliance, as seen previously in non-inertial creep. Strain is plotted against time to produce a response curve with similar overall features as in non-inertial creep, with the addition of oscillatory behavior. The oscillations mimic a specific frequency, and storage and loss properties are extracted for how the material would behave at this frequency under a sinusoidal driving force. This frequency is much higher than in the very low frequency non-inertial creep experiments. As a result, useful information can be extracted more quickly, meaning the experiments take less time. This is an appeal of inertial creep.

In inertial creep, a parameter α not seen in the non-inertial models is present. This parameter represents the inertia of the instrument. Theoretically it is a known parameter, however it is difficult to determine its value for the instrument and is therefore usually included in the list of parameters to be fit in the model. Different ringing characteristics in the responses can potentially be captured by one of several standard models which have been coupled to the inertia

of the instrument: Inertial Maxwell, Inertial Voigt and Inertial Maxwell-Jeffrey. Each model corresponds to a linear differential constitutive law which can be solved in closed form.

The models, the corresponding constitutive laws, and their solutions under a step stress are given in Section 3.3 below. The stress function is given by $\tau(t) = \tau_0 H(t - t_0)$. Solutions under a step stress rather than a top hat stress, as in Sections 2.3 and 2.4, are given here for simplicity due to the fact that inertial solutions are much longer then non-inertial solutions and top hat solutions would require twice as many terms. Additionally, one may notice that the inertial constitutive laws presented here do not contain γ - this is a result of the way in which inertial problems must be handled, which is discussed in the example derivation in Section 3.2 below.

3.2 Example: Coupling of Instrumental Inertia to Maxwell Model and Derivation of Analytical Solution

We refer to (Barav98) for a more thorough explanation on coupling viscoelasticity and instrumental inertia. Here, we give the mathematical details of how to derive the coupled constitutive law for the Two Parameter Maxwell model, followed by the steps for solving the model for the strain, given an applied step stress.

We need an equation to describe the motion of the rotating part of the rheometer. Newton's second law, given in rotational terms, is

$$I\frac{d\dot{\theta}}{dt} = \Gamma_A - \Gamma_R \tag{3.1}$$

where I is the moment of inertia of the rotating rod and cone in the machine, $\dot{\theta}$ is the angular velocity, Γ_A is the applied torque, and Γ_R is the resistive torque due to the sample. This general law can be written in terms of stress and strain as

$$\alpha\ddot{\gamma}_R = \tau_A - \tau_R \tag{3.2}$$

where $\alpha = I\frac{F_\tau}{F_{\dot\gamma}}$ is a constant, F_τ is the proportionality factor between shear stress and torque, and $F_{\dot\gamma}$ is the proportionality factor between shear rate and angular velocity. Equation (3.2) is what we wish to couple to the constitutive law for the Two Parameter Maxwell model, reprinted here,

$$\lambda\dot\tau_R + \tau_R = \eta\dot\gamma_R \tag{3.3}$$

Equation (3.2) is an equation for $\ddot\gamma$. The logic for solving this inertial problem is to substitute (3.2) into (3.3) after differentiating (3.3) once. This gives us

$$\lambda\ddot\tau_R + \dot\tau_R = \eta\left(\frac{1}{\alpha}\tau_A - \frac{1}{\alpha}\tau_R\right) \tag{3.4}$$

The goal is to eliminate γ from the equation and obtain an expression for τ_R. Once we find τ_R, we can substitute it back into Equation (3.2) to solve for γ. If we let the applied stress be a shear step stress, $\tau_A = \tau_0 H(t)$, then we have

$$\lambda\ddot\tau_R + \dot\tau_R + \frac{\eta}{\alpha}\tau_R = \frac{\eta}{\alpha}\tau_0 H(t) \tag{3.5}$$

The solution to the second order differential equation of (3.5) will have oscillating and non-oscillating regimes (that is, it will have one solution containing sines and cosines, and one containing hyperbolic sines and hyperbolic cosines). Oscillations will exist for $1^2 - 4(\lambda)(\eta/\alpha) \leq 0$, or, rearranging, for $G \leq \frac{4\eta^2}{\alpha}$ (recall $\lambda = \eta/G$). Now, when we coupled the equations we lost $\gamma(t)$, and we have remaining an equation that we wish to solve for $\tau(t)$.

To begin, we take the Laplace Transform of (3.5) and solve for $T(s)$, obtaining,

$$T(s) = \tau_0\left(\frac{\eta}{\alpha}\right)\frac{1}{s(\lambda s^2 + s + \frac{\eta}{\alpha})} \tag{3.6}$$

We use partial fractions to break up the denominator. Observe,

$$\begin{aligned}\frac{1}{s(\lambda s^2+s+\frac{\eta}{\alpha})} &= \frac{A}{s}+\frac{Bs+C}{\lambda s^2+s+\frac{\eta}{\alpha}} \\ 1 &= A\left(\lambda s^2+s+\frac{\eta}{\alpha}\right)+(Bs+C)s\end{aligned}$$

We solve for A first by letting $s=0$:

$$\begin{aligned}1 &= A\left(\lambda 0^2+0+\frac{\eta}{\alpha}\right)+(B*0+C)*0 \\ 1 &= A\frac{\eta}{\alpha} \\ A &= \frac{\alpha}{\eta}\end{aligned}$$

Next, we solve for B and C by equating coefficients of the s^2 and s terms respectively, and using $A=\frac{\alpha}{\eta}$. For s^2 we have

$$\begin{aligned}0 &= A\lambda+B \\ 0 &= \frac{\alpha}{\eta}\frac{\eta}{G}+B \\ B &= \frac{-\alpha}{G}\end{aligned}$$

Equating coefficients for s we have

$$\begin{aligned} 0 &= A+C \\ 0 &= \frac{\alpha}{\eta}+C \\ C &= \frac{-\alpha}{\eta} \end{aligned}$$

Now we can rewrite equation (3.6) as partial fractions:

$$T(s) = \tau_0 \left(\frac{\eta}{\alpha}\right) \left(\frac{\alpha/\eta}{s} + \frac{\frac{-\alpha}{G}s + \frac{-\alpha}{\eta}}{\lambda s^2 + s + \frac{\eta}{\alpha}}\right) \tag{3.7}$$

which simplifies as

$$T(s) = \tau_0 \left(\frac{1}{s} - \frac{s + G/\eta}{s^2 + (G/\eta)s + G/\alpha}\right) \tag{3.8}$$

To find the inverse Laplace Transform, we must manipulate equation (3.8) into a form for which we recognize inverses. First we split up the large fraction:

$$T(s) = \tau_0 \left(\frac{1}{s} - \frac{s}{s^2 + (G/\eta)s + (G/\alpha)} - \frac{G/\eta}{s^2 + (G/\eta)s + (G/\alpha)}\right) \tag{3.9}$$

Next we perform completing the square on the denominators:

$$\begin{aligned} T(s) &= \tau_0 \left(\frac{1}{s} - \frac{s}{s^2 + (G/\eta)s + (G/2\eta)^2 + (G/\alpha) - (G/2\eta)^2}\right. \\ &\quad \left. - \frac{G/\eta}{s^2 + (G/\eta)s + (G/2\eta)^2 + (G/\alpha) - (G/2\eta)^2}\right) \\ &= \tau_0 \left(\frac{1}{s} - \frac{s}{(s + G/2\eta)^2 + \frac{G}{\alpha} - \frac{G^2}{4\eta^2}} - \frac{G/\eta}{(s + G/2\eta)^2 + \frac{G}{\alpha} - \frac{G^2}{4\eta^2}}\right) \end{aligned}$$

Lastly, we require that the s in the numerator of the middle term be shifted by $G/2\eta$ to

match the s in the denominator. Thus, we add and subtract $G/2\eta$ to the middle term and simplify:

$$\begin{aligned} T(s) &= \tau_0 \left(\frac{1}{s} - \frac{s+G/2\eta-G/2\eta}{(s+G/2\eta)^2+\frac{G}{\alpha}-\frac{G^2}{4\eta^2}} - \frac{G/\eta}{(s+G/2\eta)^2+\frac{G}{\alpha}-\frac{G^2}{4\eta^2}} \right) \\ &= \tau_0 \left(\frac{1}{s} - \frac{s+G/2\eta}{(s+G/2\eta)^2+\frac{G}{\alpha}-\frac{G^2}{4\eta^2}} - \frac{G/2\eta}{(s+G/2\eta)^2+\frac{G}{\alpha}-\frac{G^2}{4\eta^2}} \right) \end{aligned} \tag{3.10}$$

Now we are ready to take the inverse Laplace Transform. The first term will transform back to 1, the second term is a $\cos(t)$ term, and the last term is a $\sin(t)$ term. Additionally, the cos and sin terms are shifted by $G/2\eta$, which results in an exponential term $e^{-\frac{G}{2\eta}t}$ to appear in the inverse transform. The final result is

$$\tau(t) = \tau_0 \left(1 - e^{-\frac{G}{2\eta}t} \left[\cos(\omega t) + \frac{G}{2\eta\omega} \sin(\omega t) \right] \right) \tag{3.11}$$

where $\omega = \sqrt{\frac{G}{\alpha} - \frac{G^2}{4\eta^2}}$.

Knowing τ we can now back solve for γ. We substitute equation (3.11) for τ_R and $\tau_0 H(t)$ for τ_A into equation (3.2) to find an expression for γ,

$$\ddot{\gamma}_R = \frac{\sigma_0}{\alpha} \left[H(t) - 1 + e^{-\frac{G}{2\eta}t} \left(\cos(\omega t) - \frac{G}{2\eta\omega} \sin(\omega t) \right) \right] \tag{3.12}$$

Integrating from 0 to t twice, we obtain the final solution:

$$\begin{aligned} \gamma(t) &= \frac{\tau_0}{\eta} \left[t - \frac{a}{G} \left(\frac{G}{\eta} - \frac{\eta}{a} \right) \left[1 - e^{-\frac{G}{2\eta}t} \left(\cos(\omega t) \right. \right. \right. \\ &\quad \left. \left. \left. + \frac{G}{2\eta\omega} \frac{G/\eta - 3\eta/a}{G/\eta - \eta/a} \sin(\omega t) \right) \right] \right] \end{aligned}$$

3.3 List of Inertial Models

The Inertial Maxwell Model

Constitutive Law

$$\eta\ddot{\tau} + G\dot{\tau} + \frac{\eta G}{a}\tau = \frac{\eta G}{a}\tau_0 H(t - t_0)$$

Solution in Creep

$$\begin{aligned}\gamma(t) &= \frac{\tau_0}{\eta}H(t-t_0)\left[(t-t_0) - \frac{a}{G}\left(\frac{G}{\eta} - \frac{\eta}{a}\right)\left[1 - e^{-\frac{G}{2\eta}(t-t_0)}\left(\cos(\omega(t-t_0))\right.\right.\right. \\ &\quad \left.\left.\left. + \frac{G}{2\eta\omega}\frac{G/\eta - 3\eta/a}{G/\eta - \eta/a}\sin(\omega(t-t_0))\right)\right]\right]\end{aligned}$$

where $\omega = \sqrt{\frac{G}{a} - \frac{G^2}{4\eta^2}}$.

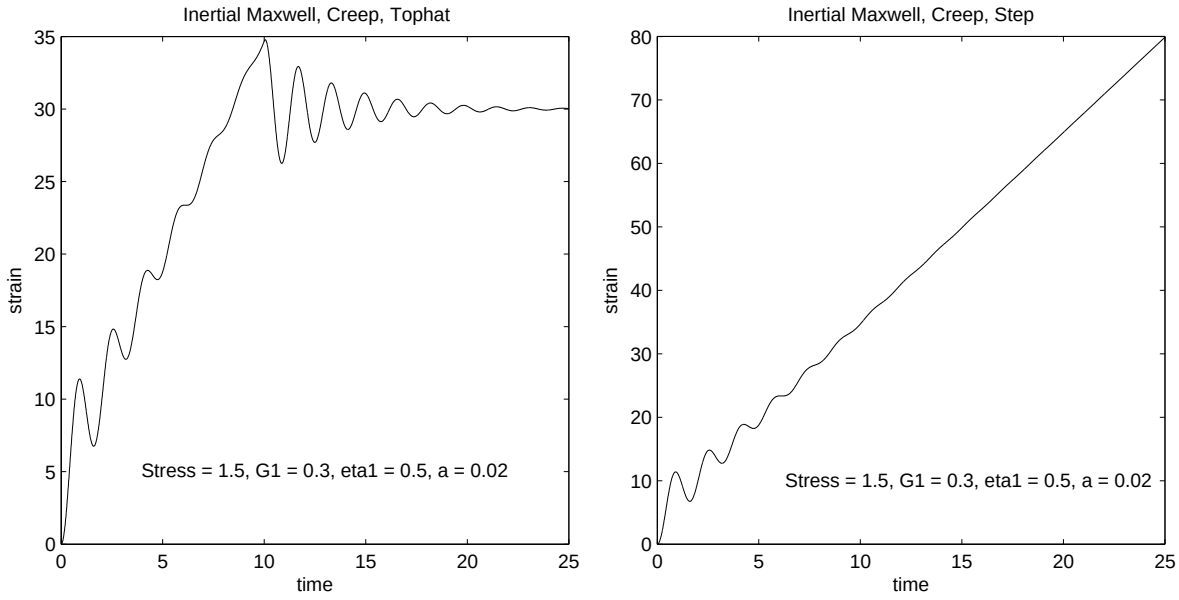

Figure 3.1: The Inertial Maxwell Model under a top hat (left) and step (right) stress.

The Inertial Kelvin-Voigt Model

Constitutive Law $\quad a\ddot{\tau}+\eta\dot{\tau}+G\tau = G\tau_0 H(t-t_0)+\eta\tau_0\delta(t-t_0)$

Solution in Creep

$$\gamma(t) \quad = \quad \frac{\tau_0}{G}H(t-t_0)\left[1-e^{-\frac{\eta}{2a}(t-t_0)}\left(\cos(\omega(t-t_0))+\frac{\eta}{2a\omega}\sin(\omega(t-t_0))\right)\right]$$

where $\omega = \sqrt{\frac{G}{a}-\left(\frac{\eta}{2a}\right)^2}$

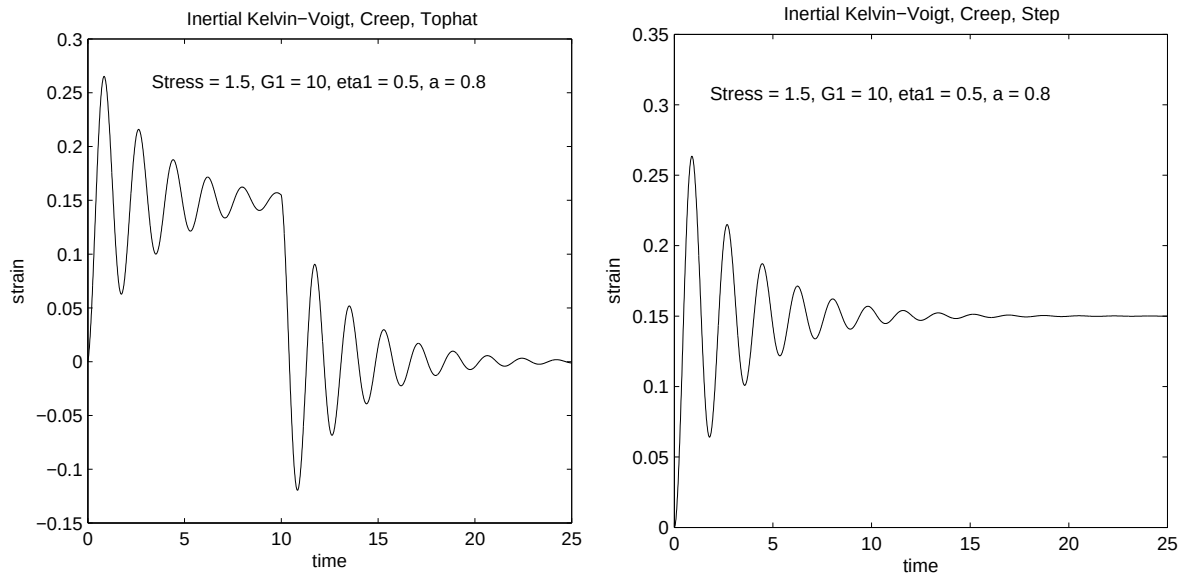

Figure 3.2: The Inertial Voigt Model under a top hat (left) and step (right) stress.

The Inertial Maxwell-Jeffrey Model

Constitutive Law

$$(\eta_1+\eta_2)\ddot{\tau}+(G+\frac{\eta_1\eta_2}{a})\dot{\tau}+\frac{G\eta_2}{a}\tau \;=\; \frac{G\eta_2}{a}\tau_0 H(t-t_0)+\frac{\eta_1\eta_2}{a}\tau_0\delta(t-t_0)$$

Solution in Creep

$$\gamma(t) \;=\; \tau_0 H(t-t_0)\left[\frac{t-t_0}{\eta_2}-B+e^{-A(t-t_0)}\left(B\cos(\omega(t-t_0))+\frac{A}{\omega}(B-\frac{1}{A\eta_2})\sin(\omega(t-t_0))\right)\right]$$

where $\omega=\sqrt{\frac{\eta_2 G}{a(\eta_1+\eta_2)}-A^2}$, $A=\frac{aG+\eta_1\eta_2}{2a(\eta_1+\eta_2)}$, and $B=\frac{a(\eta_1+\eta_2)}{\eta_2 G}\left(\frac{2A}{\eta_2}-\frac{1}{a}\right)$.

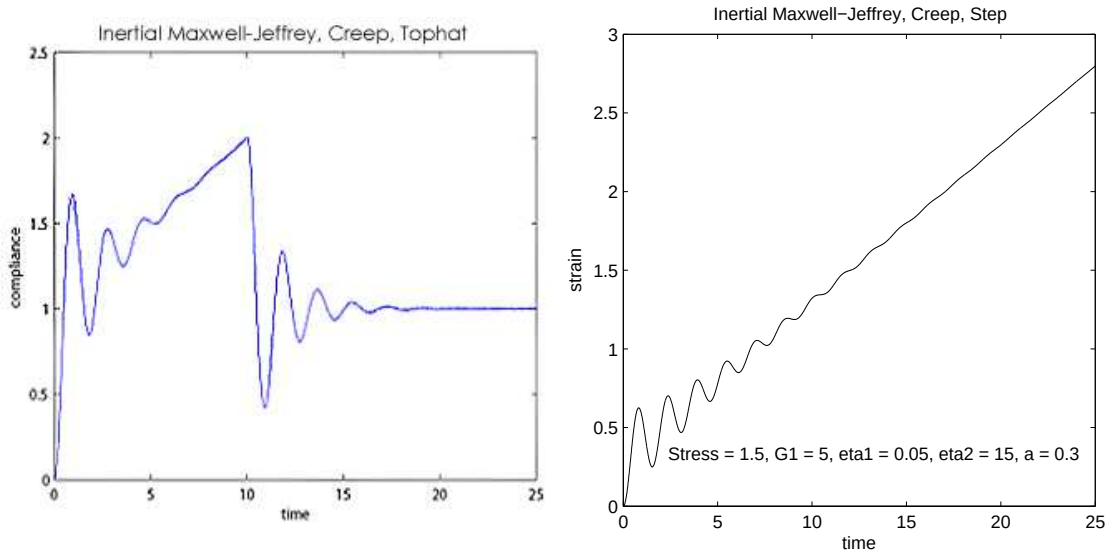

Figure 3.3: The Inertial Maxwell-Jeffrey Model under a top hat (left) and step (right) stress.

3.4 Summary of Model Signatures of Inertial Creep Experiments

Follow this guide to help choose the best inertial model to fit to your data taken under either a top hat stress or a step stress. Refer to the figures above for examples of each model, and see Section 4.2 for demonstrations of how each is used to fit experimental data. Note that the items to distinguish between the inertial models are essentially the same (after considering the oscillations) as the non-inertial models. Note also that the Inertial Maxwell and Inertial Maxwell-Jeffrey models are identical in graphical behavior, whereas in the non-inertial regimes the models from which these are derived are quite different. Because of this similarity, there are essentially only two inertial graphs given here to choose from, and thus only one feature is required to distinguish the two. Two separate features are given here, the first dealing with end behavior and the second dealing with the transition when stress is turned off. These two features rely heavily on the distinction between liquid-like and solid-like behavior, as there are no intermediate options having a mix of characteristics (as in the Two Parameter Voigt model for the non-inertial options).

1. Look at the terminal behavior of the response curve for your material. In step stress, does it level off at some finite steady state value? In top hat stress, does it recover to zero?

   (a) If yes, try the **Inertial Kelvin-Voigt** model. The material exhibits solid-like behavior.

   (b) If the oscillations have an overall positive slope in step stress, or recover to a positive steady state in top hat stress, try either the **Inertial Maxwell** or the **Inertial Maxwell-Jeffrey** model. These are liquid-like behaviors.

2. In a top hat stress, does the curve make a sudden jump when the stress is suddenly

removed?

(a) If the oscillations jump from one baseline value down to zero at the time when the stress is turned off (a solid-like behavior), try the **Inertial Kelvin-Voigt** model.

(b) If the oscillations switch from steadily increasing to leveling off around some non-zero value (no sudden jump is a liquid-like behavior), try either the **Inertial Maxwell** or the **Inertial Maxwell-Jeffrey** model.

Chapter 4

Software Tools

4.1 Parameter Inference and Analysis of Parameters Using Mathematica

Each model discussed in this thesis has either two or three fundamental parameters that completely determine the final shape of the curve. The parameters are chosen from G_1, G_2, η_1, or η_2. For a given model, it is expected that each parameter may have a strong effect on the shape of the curve (that is, changing the value of this parameter by small amounts causes larger changes to the shape) or may have only a weak affect on the shape of the curve (the curve will look similar across a wide range of values for this parameter). Knowing which parameters have strong and weak affects may help in analyzing the parameter fittings of experimental data. For example, it may influence the decision of when to hold a known value constant versus when to let it iterate.

To get an idea of how each parameter affects the shape of a given model, Mathematica can be used to create dynamic plots of each model. The function 'Manipulate' is used in conjunction with 'Plot' to create a graph of the model along with slider bars for each parameter in the model. The graph changes as the sliders are altered. The code for this is only two lines. The first defines the equation and the second calls 'Manipulate' and defines ranges for each

slider.

```
Function_Name[param1_, ... ] := equation
Manipulate[Plot[Function_Name[parameters],{t,0,20},PlotRange
    ->{0,5}],{Param1,min,max},...]
```

For example, to generate a dynamic plot of the compliance for the Two Parameter Voigt model, the following can be used:

```
CRVoigt2[G_, n_] := (1/G)*(UnitStep[t]*(1 - Exp[-(t*G)/n]) -
    UnitStep[t - tend]*(1 - Exp[-((t - tend)*G)/n]))
Manipulate[Plot[CRVoigt2[G, eta], {t, 0, 20}, PlotRange -> {0,
    1.5}], {G, 0, 5}, {eta, 0, 5}]
```

After adjusting the parameter values, the output will look similar to Figure 4.1 below.

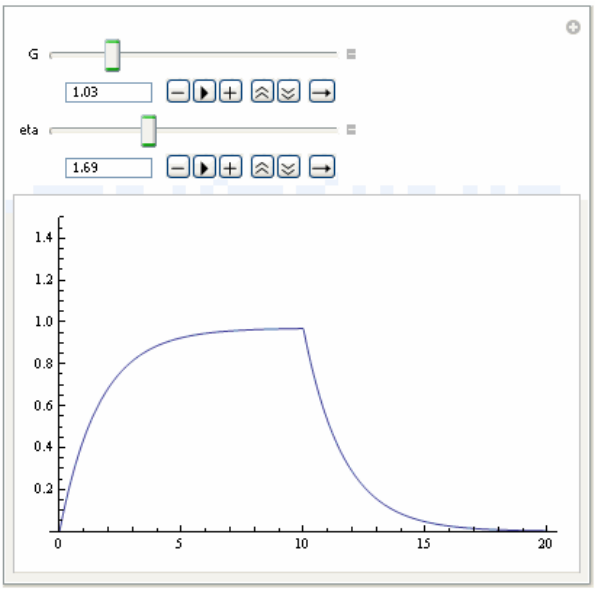

Figure 4.1: A screen shot of the Manipulate function in Mathematica applied to plotting the Two Parameter Voigt model with dynamic parameters.

Parameter sensitivity is affected by values of other parameters

Through observation, it is found that the effects of a parameter on the graph depend on several factors. First, characterizing the effects of a parameter depends on whether the parameter is in a high or low regime as well as whether the remaining parameters are at high or low values. Consider the Three Parameter Voigt model,

$$\gamma(t) = \frac{1}{G_2}H(t-t_0)\left[\frac{G_1+G_2}{G_1} - \frac{G_2}{G_1}e^{-\frac{(t-t_0)G_1}{\eta}}\right] - \frac{1}{G_2}H(t-t_1)\left[\frac{G_1+G_2}{G_1} - \frac{G_2}{G_1}e^{-\frac{(t-t_1)G_1}{\eta}}\right]$$

We observe that η, which is seen in the denominator of the exponential, affects the sharpness of the curve - smaller values of η cause a larger exponent and generate a steeper curve. The parameter G_1 is also related to the exponent, as well as the magnitude of the entire curve. Thus, when η is very small (leading toward a sharp curvature), small values of G_1 counteract η and lead to a more gradual curvature. In this realm, small changes in G_1 can cause the curve to look very different. For $\eta = 2$ and $G_2 = 2$, compare the curves in Figure 4.2 when G_1 changes from 0.5 to 1.5, a step of one unit.

On the other hand, when G_1 is larger than η, it amplifies the effect that η already has on the graph and produces a very steep initial rise followed by a sudden flattening out. In this realm (small η, large G_1), the ratio $\frac{G_1}{\eta}$ is already so large that even large changes in G_1 have a very small effect on the overall shape of the curve. For $\eta = 2$ and $G_2 = 2$, compare the curves in Figure 4.3 when G_1 changes from 20 to 30, a step of 10 units.

This interaction between parameters can be explained by realizing that, in each model, the pieces that really affect the shape of the graph are functions of the basic parameters G_1, G_2, η_1 or η_2. As a simple example, consider the equation of a line, $y = mx + b$. Here, m defines the slope and b defines the y-intercept. However, if you are concerned with two different parameters, say h and g, where $y = \frac{h}{g}x + h$, then the slope is no longer defined by a single parameter. The linear viscoelastic models considered here are for the most part more complicated than a

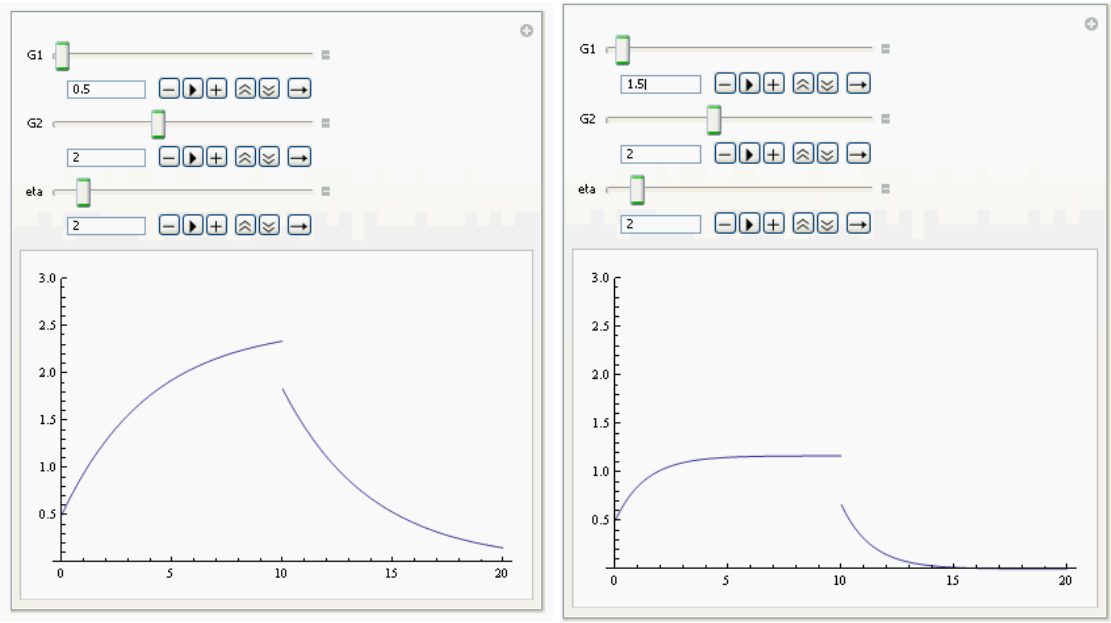

Figure 4.2: The Three Parameter Voigt model changes noticeably for small changes in G_1 when G_1 is small compared to η.

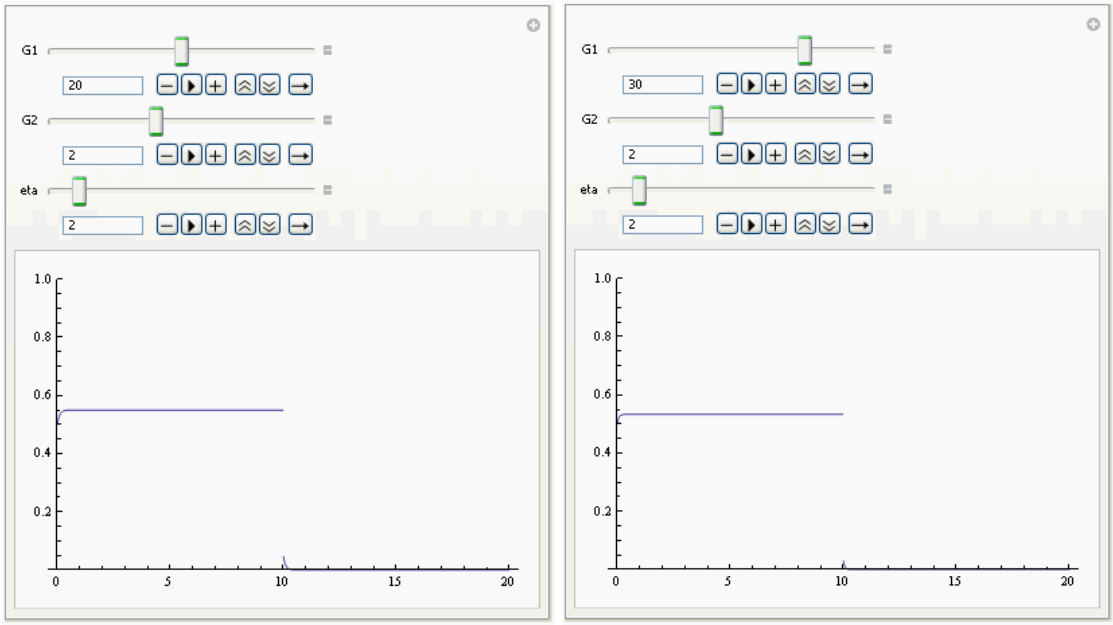

Figure 4.3: The Three Parameter Voigt model changes very little for changes in G_1 when G_1 is large compared to η.

simple line, and thus the interactions between parameters are even more intricate.

Parameter analysis is affected by which graphical features are important

Parameter sensitivity also depends on what features of the graph are important for analyzing the data. For instance, in fluid models often the slope of the compliance curve after a long time step stress or the value to which the fluid recovers after stress is removed are important indicators of the viscosity of the fluid. If this is all that needs to be observed from the data, then any parameters not directly affecting the long time slope may be unimportant. It could be said that these parameters are not sensitive to the prediction of the viscosity. However, any parameters affecting the end behavior will need to be considered more closely.

The Maxwell-Jeffrey model is a linear viscoelastic fluid model which exhibits a constant slope in long times while constant stress is applied, and recovers to a positive steady state after the removal of stress. It can easily be observed using Mathematica that out of the three parameters creating the Maxwell-Jeffrey model, G, η_1 and η_2, only η_2 changes the long time end behavior. This is verified by looking at the equation,

$$\begin{aligned}\gamma(t) &= \frac{1}{G}\left[H(t-t_0)-H(t-t_1)\right]+\frac{1}{\eta_2}\left[(t-t_0)H(t-t_0)-(t-t_1)H(t-t_1)\right] \\ &\quad -\frac{1}{G}\left[H(t-t_0)e^{-\frac{(t-t_0)G}{\eta_1}}-H(t-t_1)e^{-\frac{(t-t_1)G}{\eta_1}}\right]\end{aligned}$$

and noticing that η_2 is the only parameter affecting the second term, which is the only term that does not go to zero as t increases. The larger η_2 is, the smaller the slope and/or steady state value of the end behavior. Thus, if you are trying to model this end behavior, you will need to estimate η_2 to high accuracy while the other parameters could be allowed to vary greatly.

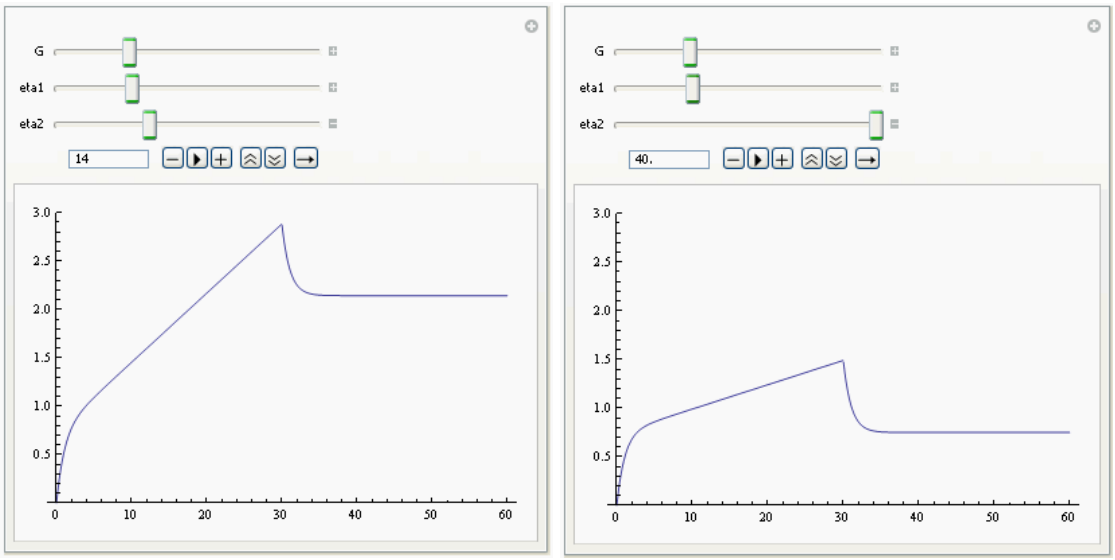

Figure 4.4: For $\eta_2 = 14$ (left figure), the slope of the end behavior (as well as the steady state value) are much higher than for $\eta_2 = 40$ (right figure). G affects the overall magnitude of the stress-on part of the graph, and η_1 affects the curvature, but neither G nor η_1 affects end behavior.

Parameter inference is influenced by the fitting region

During the fitting process, parameter sensitivity is also influenced by the size of the region you are fitting to, and which particular features are captured in this region. The region must be large enough to capture some defining features of the data, but must be small enough to prevent the fitting algorithm from crashing. That is, you cannot always simply fit over the entire domain of the data. It is important to consider these two things (length and position of fitting interval) because parameters do not affect all regions of a graph in the same way.

Reconsider the Maxwell-Jeffrey model. In the table below, large error bars were introduced to the Maxwell-Jeffrey model having the true parameters $G = 1$, $\eta_1 = 2$, and $\eta_2 = 12$ to try to determine how much random error could be present while still predicting accurate parameter values. Data was generated for 10%, 30% and 50% random error, and the parameter_fitting_gui from (Xu2009) was used to recover the parameters in the interval $t = (0,5)$.

It can be seen that η_2 deviates most from its true value of 12. Now, recall the discussion

% Err / True Parameters	.1%	.3%	.4%
G = 1	0.92	1.35	1.46
Eta_1 = 2	1.99	2.13	1.98
Eta_2 = 12	14.05	7.74	7.27

Figure 4.5: Even at 50% random error, G and η_1 remain close to their true values of 1 and 2, respectively. However, η_2 deviates, likely due to the early fitting window.

in the previous section. We have demonstrated that η_2 is responsible for changing the end behavior. However, the fitting interval $(0,5)$ does not include information on the end behavior. That is, a good fit can be made in $(0,5)$ for a range of values of η_2 because changes in η_2 do not affect this part of the graph. Figure 4.6 demonstrates how values of η_2 from 8 to 15 do not change the fitting region very greatly.

Related to this issue is the usage of fitting intervals which are too small. The same Maxwell-Jeffrey model with parameters $G = 1$, $\eta_1 = 2$, and $\eta_2 = 12$ was fit in the small interval $t = (7,8)$. This returned parameter estimates of $G^* = 0.012$, $\eta_1^* = -0.678$, and $\eta_2^* = 0.558$. Figure 4.7 shows how the the two models align very closely on the interval $(7,8)$; however, the model generated by G^*, η_1^* and η_2^* is vastly different from the original data, as Figure 4.8 shows.

4.2 Generating Experimental Error: Make_Data Tool

The data obtained from creep experiments is expected to be nonlinear, which can be supported by the observation of parameter walk-offs, as demonstrated in (Xu2009). Thus, these linear models cannot be expected to match the data exactly. In addition, experimental data is noisy, and this may interfere with the fitting algorithm. To examine whether simple random error could be added to an exact model to reflect the noise in raw data, we added functionality to the parameter_fitting_gui from (Xu2009) which allows a user to choose a model, enter a value

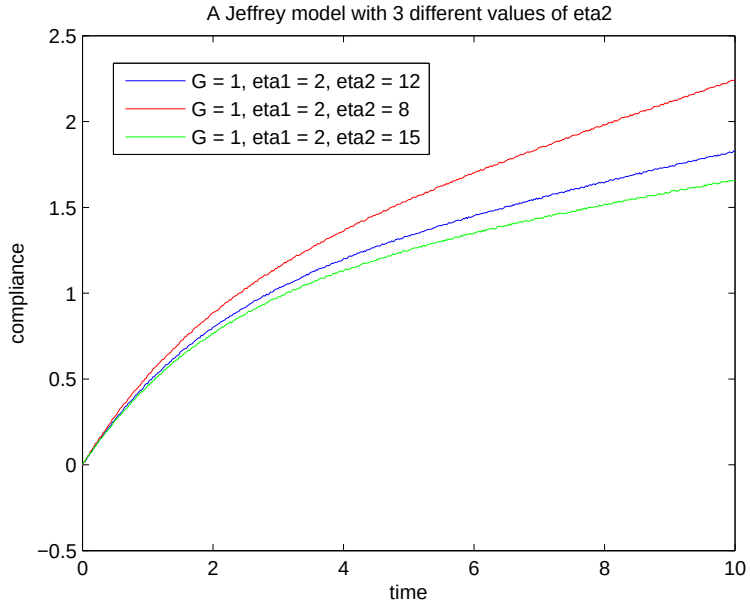

Figure 4.6: Observe that the three graphs, created by varying η_2 between 8 and 15 and holding the other parameters constant, are slow to spread out. This means that the closer the fitting interval is to 0, the better any value of η_2 between 8 and 15 could generate a reasonable fit.

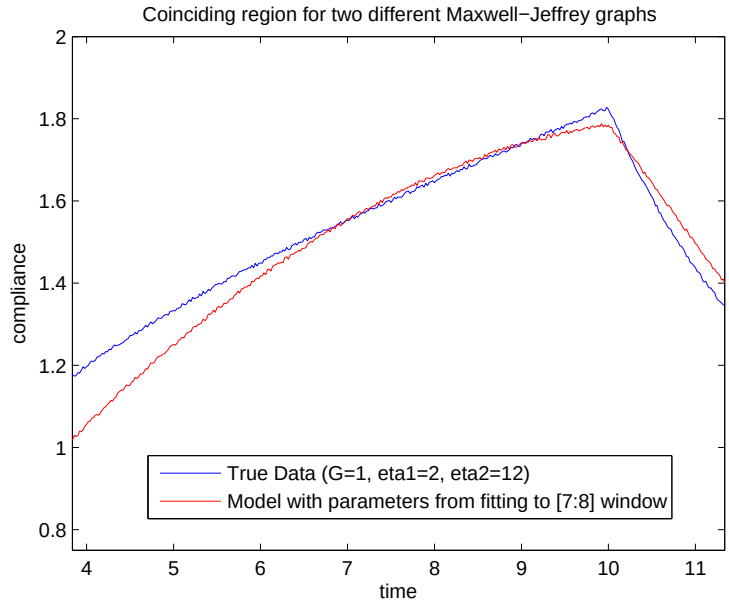

Figure 4.7: On the fitting interval (7,8), the predicted parameters give a well aligned graph. However, they do not do well to portray the rest of the data.

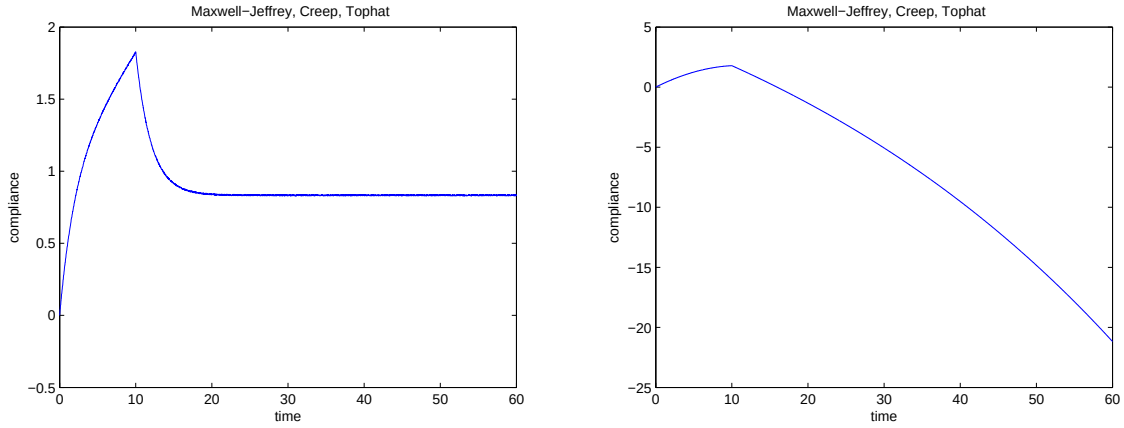

Figure 4.8: The original data on the left was fit to a Maxwell-Jeffrey model on the small interval $t = (7, 8)$. The resulting poorly fit parameters were used to create the very different model on the right.

for each parameter, enter the desired percentage of random error, and generate data based off these selections. Thus, the user can work with data with known parameters to test how well the parameter_fitting_gui software is able to recover those values despite the presence of noise.

This make_data environment is shown in Figure 4.9. It can be accessed directly through Matlab by typing 'guide' in the command window and opening 'make_data.fig'. It can also be accessed through the parameter_fitting_gui by pressing the button labeled 'Create Exact Data'. The user selects one of the models discussed in this thesis from the drop down menu at the top. The related equation is displayed in the dark shaded box below the drop down menu. To the right of the displayed equation is a box labeled 'Parameter Values' (Figure 4.10), in which only the appropriate parameters for the chosen model will be enabled. The user must enter numerical values for each parameter.

The bottom left box is labeled 'Set Details of Applied Stress Function' (Figure 4.11). Here the user can enter a value for the percent error and can select between three types of applied stress (step, top hat or periodic top hat). If 'Periodic Top Hat' is selected, then a value for 'dx' must be entered, which is the length between applied stress intervals. The user must also enter the 'Force On Time' (time at which the stress is applied), 'Force Off Time' (time at which the

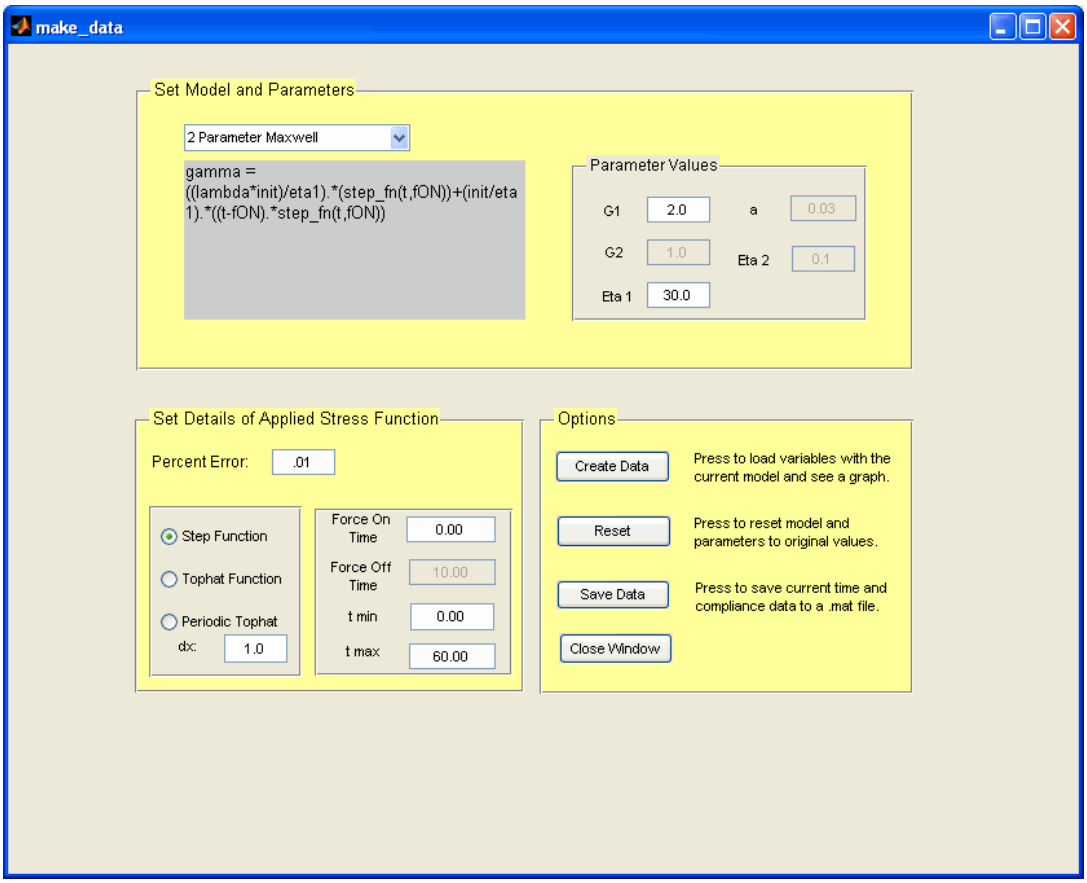

Figure 4.9: This make_data environment was added to the parameter_fitting_gui from (Xu2009) to allow users to generate data with known parameter values and a chosen amount of random error.

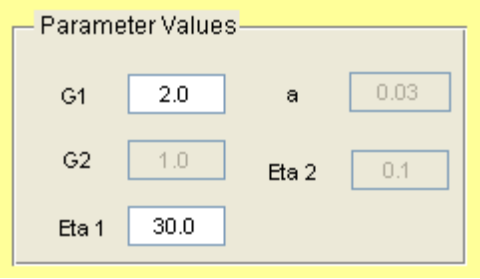

Figure 4.10: Close up of 'Parameter Values' box in make_data.fig.

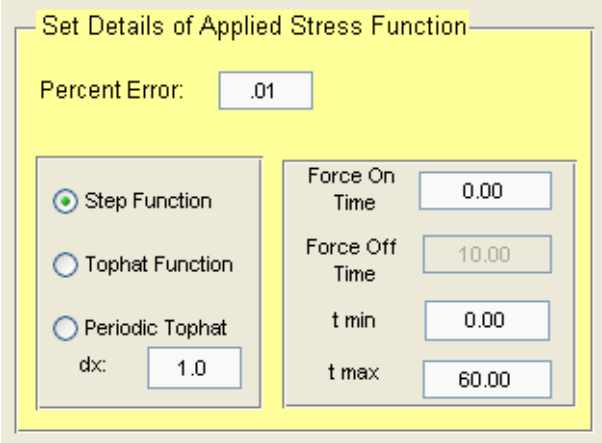

Figure 4.11: Close up of 'Set Details of Applied Stress Function' box in make_data.fig.

stress is turned off), and 'tmin' and 'tmax' (the graphing domain).

In the bottom right box labeled 'Options' (Figure 4.12), the user can press 'Create Data' to see a graph of the current selections. Pressing 'Reset' will reopen the make_data environment

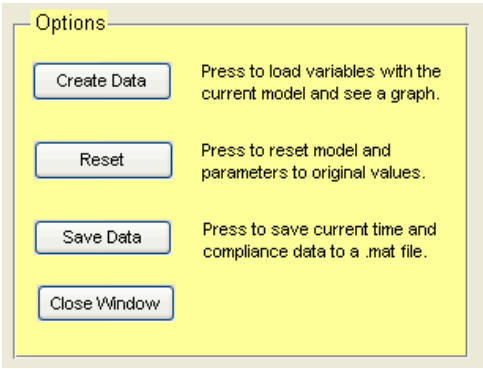

Figure 4.12: Close up of 'Options' box in make_data.fig.

with all of the selections returned to the preset values. The user should press 'Save Data' when the desired model is obtained. This will create a .mat file containing the time vector stored as the t variable and the compliance vector stored as the x variable, which is the format required to be compatible with the parameter_fitting_gui. The user is allowed to enter a name for the .mat file. At this point, pressing 'Close' will close the make_data window and allow the user to continue analyzing the data in the parameter_fitting_gui.

Sample experimental data was examined to estimate the typical percentage of error, which is assumed here to be experimental error. This value was estimated to be about 1%. This is the preset value displayed when opening the window, but the user can enter any amount of error desired. A vector of random numbers from -0.5 to 0.5 is generated and multiplied by the chosen error percentage. This vector is then added to the exact data to convert it to noisy data.

The example fitting in Figure 4.13 of the Three Parameter Voigt model to data having 5% error demonstrates how the fitting algorithm is able to overcome the random noise and generate a curve that seems to fit well with the true data. This observation that the random noise does not interfere heavily with the fitting algorithm is supported by a small study of fittings across a range of models. The table in Figure 4.14 summarizes the trials. For the Two Parameter Voigt model, the input parameters are η and G and the returned fitted parameters are J and D. The conversion is given by $G = \frac{1}{J}$, $\eta = D$. For the Maxwell-Jeffrey model, the input parameters are G, η_1 and η_2, and these parameters are also returned by the fitting software. In the parameter_fitting_gui the Three Parameter Voigt model is listed as the 'Linear Solid' model, and the parameters returned are J_1, J_2 and τ. These are converted to the parameters G_1, G_2 and η by $G_1 = \frac{1}{J_2}$, $G_2 = \frac{1}{J_1 - J_2}$, $\eta = \frac{\tau}{J_2}$.

Several sets of parameters were chosen for each model to try to obtain a wide range of graphical features. Error was increased from 0.1% to 5.0%. The results indicated that the values being predicted by the fitting algorithm closely matched the true parameter values across all tested levels of error. There did not seem to even be a strong trend in the decrease in accuracy as the error was increased. It seems as if the error in the predicted parameter values is random. Consider Figures 4.15 showing the error in parameters G and η_1 for the Maxwell-Jeffrey model for 1%, 2%, 3%, 4% and 5% error. The error in predicting G seems to increase; however, the error in predicting η_1 jumps and then begins to decrease.

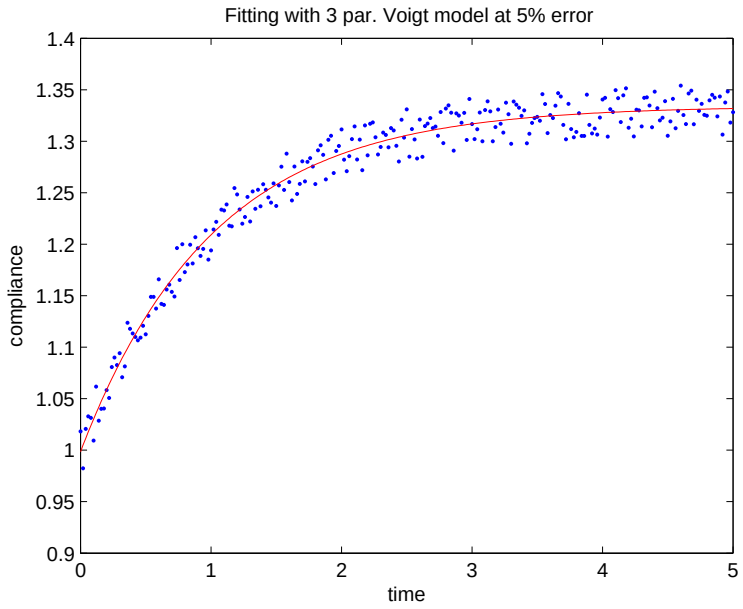

Figure 4.13: Demonstration of fitting algorithm on data with 5% error.

Summary of Controls for Error Testing

Each set done across .001, .005, .01, .03 and .05 error percentages		2 Par. Voigt	Max-Jeff	3 Par. Voigt
Set 1	G1	7	0.8	3
	Eta1	15	1	3
	G2	-	-	1
	Eta2	-	10	-
Set 2	G1	0.2	12	7
	Eta1	2	16	25
	G2	-	-	7
	Eta2	-	33	-
Set 3	G1	10	3	0.5
	Eta1	50	3	5
	G2	-	-	1
	Eta2	-	52	-

Figure 4.14: Summary of controls tested to examine influences of experimental error.

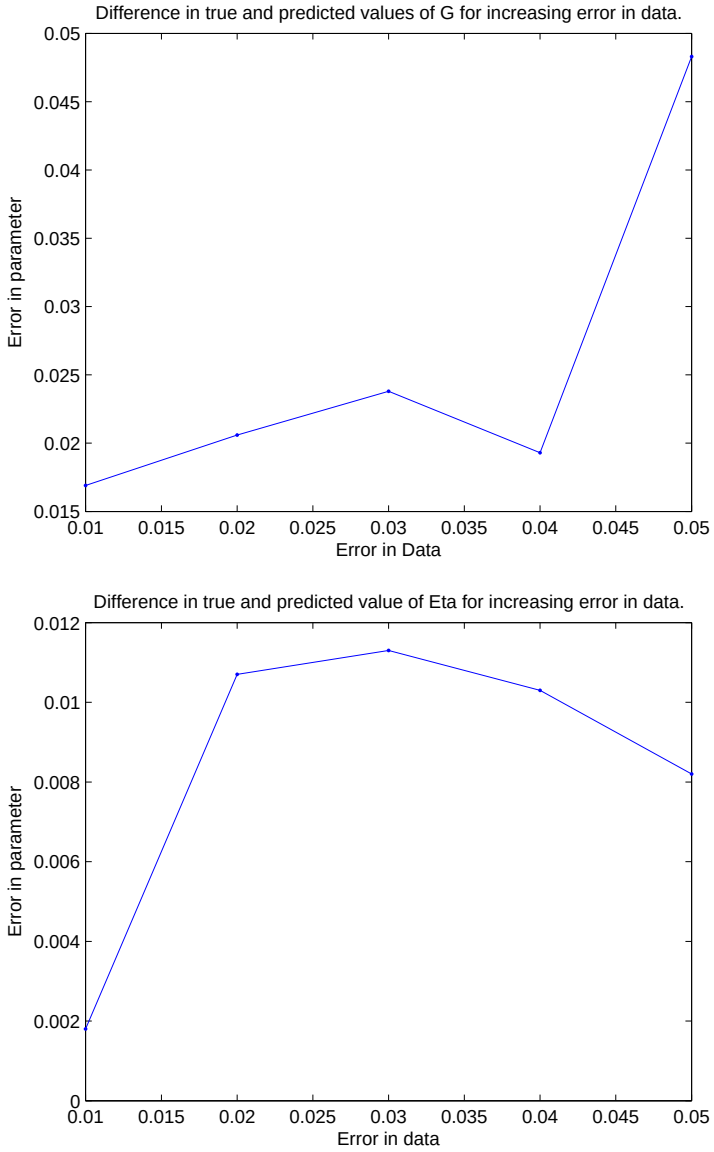

Figure 4.15: Error in predictions for parameters G and η.

4.3 Experimental Parameter Fittings after Identification of Key Signatures

Once experimental data has been collected and examined, software created by Dr. Ke Xu can be used to obtain a best fit of the parameters of a given function to the data. Additional functionality and minor edits have been made to her software and are described here, but please see (Xu2009) for further notes on the usage of this program. In this section we shall examine several sets of experimental data for the features discussed in this thesis to determine which model has the most potential for fitting the data. We will then demonstrate the results of applying the chosen model to the data.

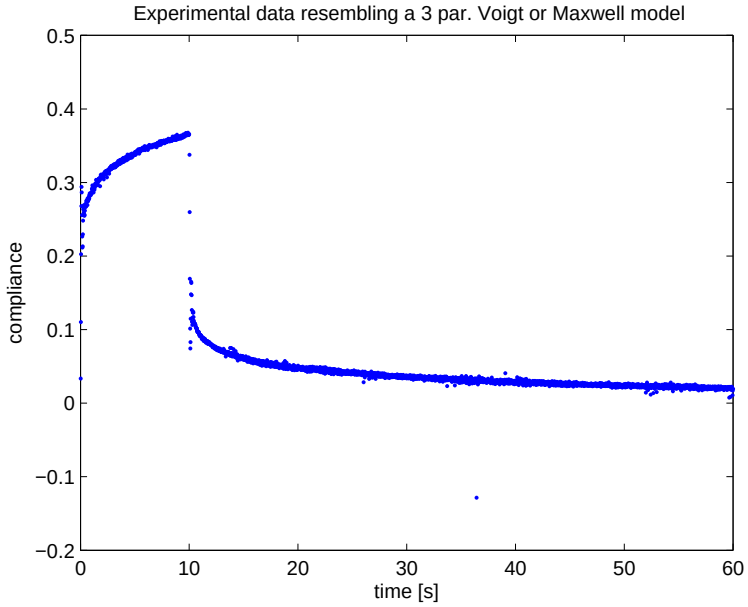

Figure 4.16: This experimental data could be modeled by the Three Parameter Maxwell or Voigt models.

Consider the agarose data in Figure 4.16 above. Although this data may not fully recover to 0, it comes close. It could be identified as a Three Parameter Maxwell or Voigt model (recall both have the same general equation and overall features). In the parameter_fitting_gui these

models are combined as the Linear Solid model. Using the Linear Solid model to fit the data on the interval $(0,5)$ the results seem close, but clearly the predicted model does not fit as well as it could (see Figure 4.17). Notice that in the first few data points of this experiment there is odd behavior resembling high frequency oscillations that are only apparent when zooming in. This behavior seems out of place with the rest of the data. As described earlier, sometimes a small amount of initial oscillation will be present unintentionally and is usually ignored. By fitting to the window $(1,5)$ instead, this fitting becomes much nicer. The user must be careful to fully consider the data at hand before applying the software.

The next three data sets we will examine are made from 0.3% agarose solutions with increasing stress levels. Agarose is known to be a highly entangled and complicated material that can be difficult to fit. As the stress is increased, we can see the data progress from a more solid-like material to a more liquid-like material. We have said that in a linear response, the compliance should remain unchanged as stress is increased. Thus, the rather good fits with linear models despite the solid to liquid changes apparent in this data are indications of stress softening, a stress-induced change in the material response. Again we observe high frequency oscillations within the first half second of data which will be ignored.

At low stress, the data appears to follow a Three Parameter Maxwell or Voigt model (recall that both behave in the same way). At the highest stress, the data appears to better follow the Maxwell-Jeffrey model. Each data set will be fit to both the Linear Solid and Maxwell-Jeffrey models for comparison of R^2 values (measuring how well the model fits the data points, also returned by the software). Each will also be fit on the interval $(1,60)$. For these simple models it is easy to fit over a large interval, and we want to be able to capture information about the entire data set. For inertial data it is best to fit in small windows.

The agarose data at the lowest stress level, 0.05 Pascals, is shown in Figure 4.18 below. It seems to have an initial jump at the onset of stress, a sudden drop when the stress is removed, and although it may not recover completely to 0, it does come very close. These are all solid-

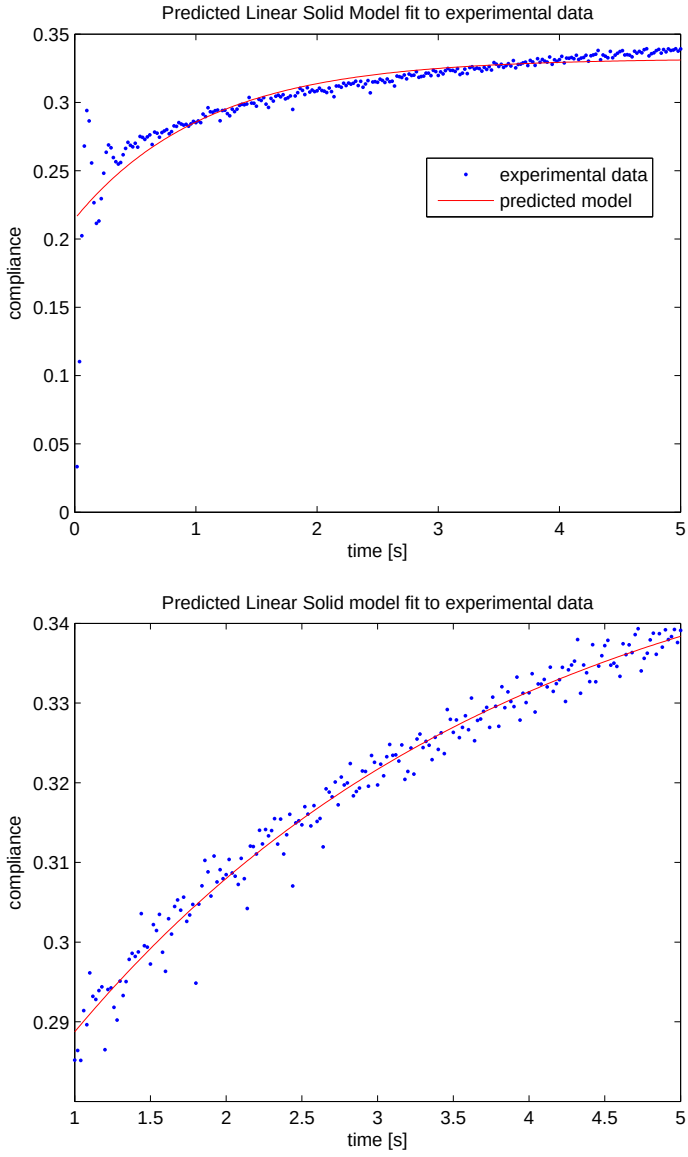

Figure 4.17: Only 1 second in the fitting interval made the difference between getting a poor fit versus a good fit.

like features captured by the Three Parameter Voigt model. The Linear Solid and Maxwell-Jeffrey fits are shown in Figure 4.19. For Maxwell-Jeffrey, $R^2 = .977$ and for Linear Solid, $R^2 = .99$, so Linear Solid has a better fit. The Linear Solid model appears to be better able to capture the slow decline toward 0 compliance, which the Maxwell-Jeffrey model attempts to find an average steady state value.

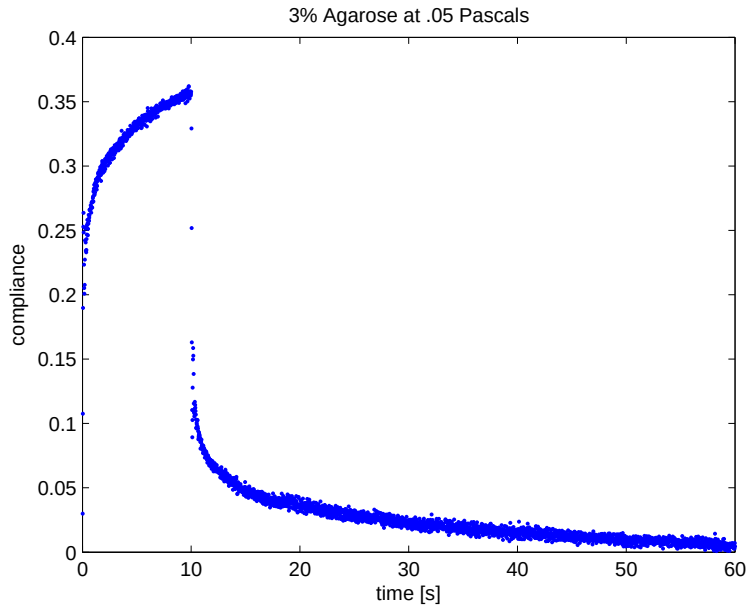

Figure 4.18: Agarose data at 0.05 Pascals having solid-like features.

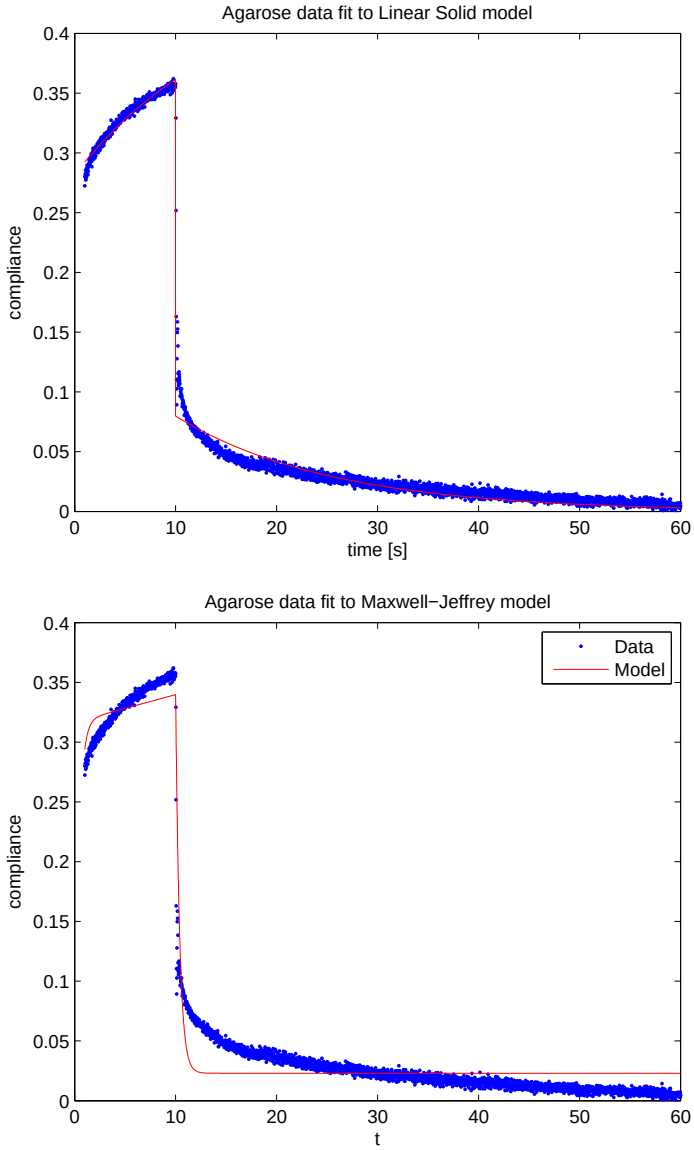

Figure 4.19: Agarose at 0.05 Pascals fit to Linear Solid and Maxwell-Jeffrey.

The agarose data at 0.2 Pascals is shown in Figure 4.20 below. It now takes on a more fluid-like quality, having a very linear increase and recovering to a value much higher than 0. These features seem best captured by the Maxwell-Jeffrey model. The Linear Solid and Maxwell-Jeffrey fits are shown in Figure 4.21. For Maxwell-Jeffrey, $R^2 = .97$ and for Linear Solid, $R^2 = .98$. Thus, though the difference is small, the Linear Solid model continues to provide a decent fit. This is surprising since the Linear Solid model must recover to 0 and the data clearly does not reach zero in this time frame. Looking closely we notice that the Linear Solid model does continue to decrease, but at such a slow rate that it appears to level out.

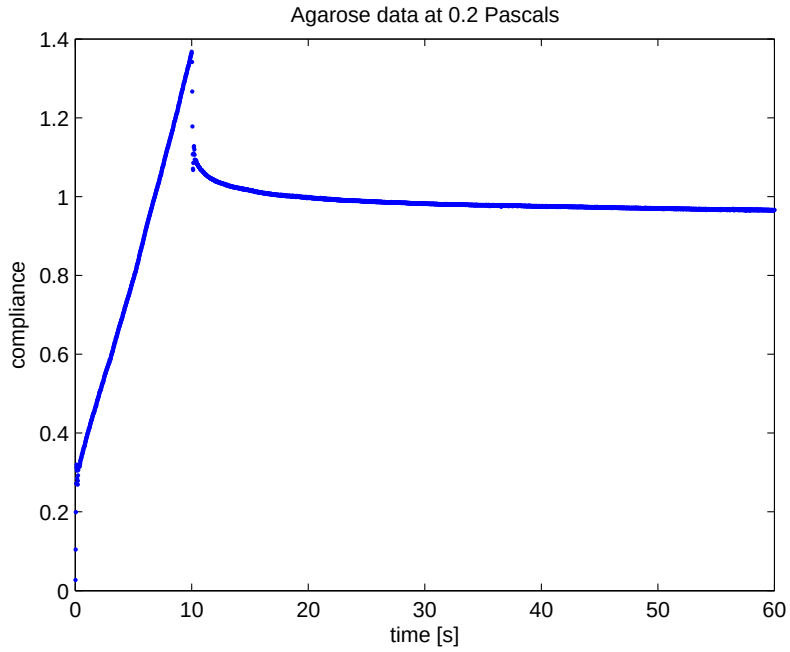

Figure 4.20: Agarose data at 0.2 Pascals having liquid-like features.

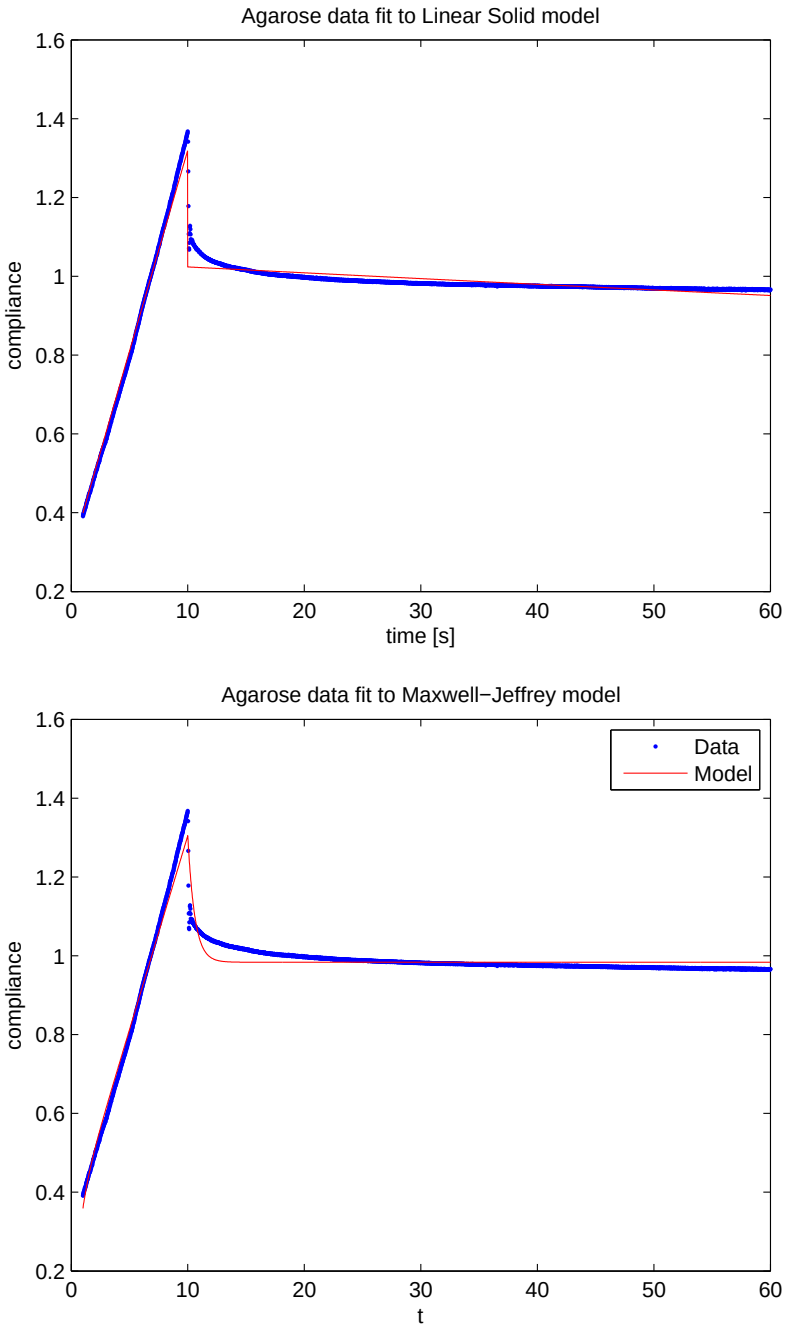

Figure 4.21: Agarose at 0.2 Pascals fit to Linear Solid and Maxwell-Jeffrey.

The agarose data at the highest stress level, 0.5 Pascals, is shown in Figure 4.22 below. It is very similar to the data at 0.2 Pascals, but more extreme. The Linear Solid and Maxwell-Jeffrey fits are shown in Figure 4.23. For Maxwell-Jeffrey and for Linear Solid, $R^2 = .99$. At this extreme, the end behavior of the data is flat enough that the Maxwell-Jeffrey model fits it very well.

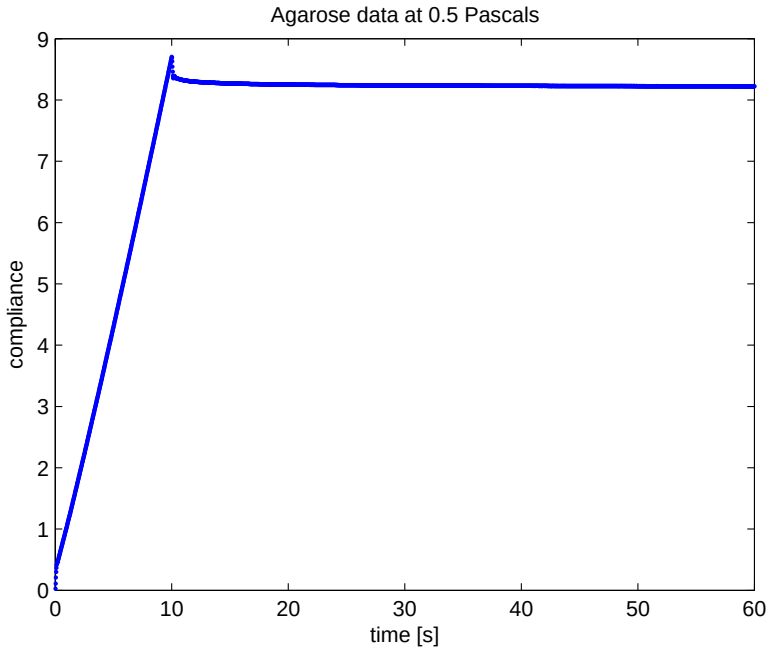

Figure 4.22: Agarose data at 0.5 Pascals having liquid-like features.

Lastly, we wish to demonstrate the difficulties in fitting to inertial data. Attempting to fit over intervals as large as used previously will cause the program to crash. This is because the regression function will be unable to converge on a best fit. Fitting over smaller windows will return good fits on the interval, but a poor overall fit to the rest of the data. Further, fitting on successive intervals will return parameter values which evolve in time. This is evidence of thixotropy - the time dependent change in the material, reflected by the need of differing parameters to accurately model different time intervals. These results are also illustrated in (Xu2009).

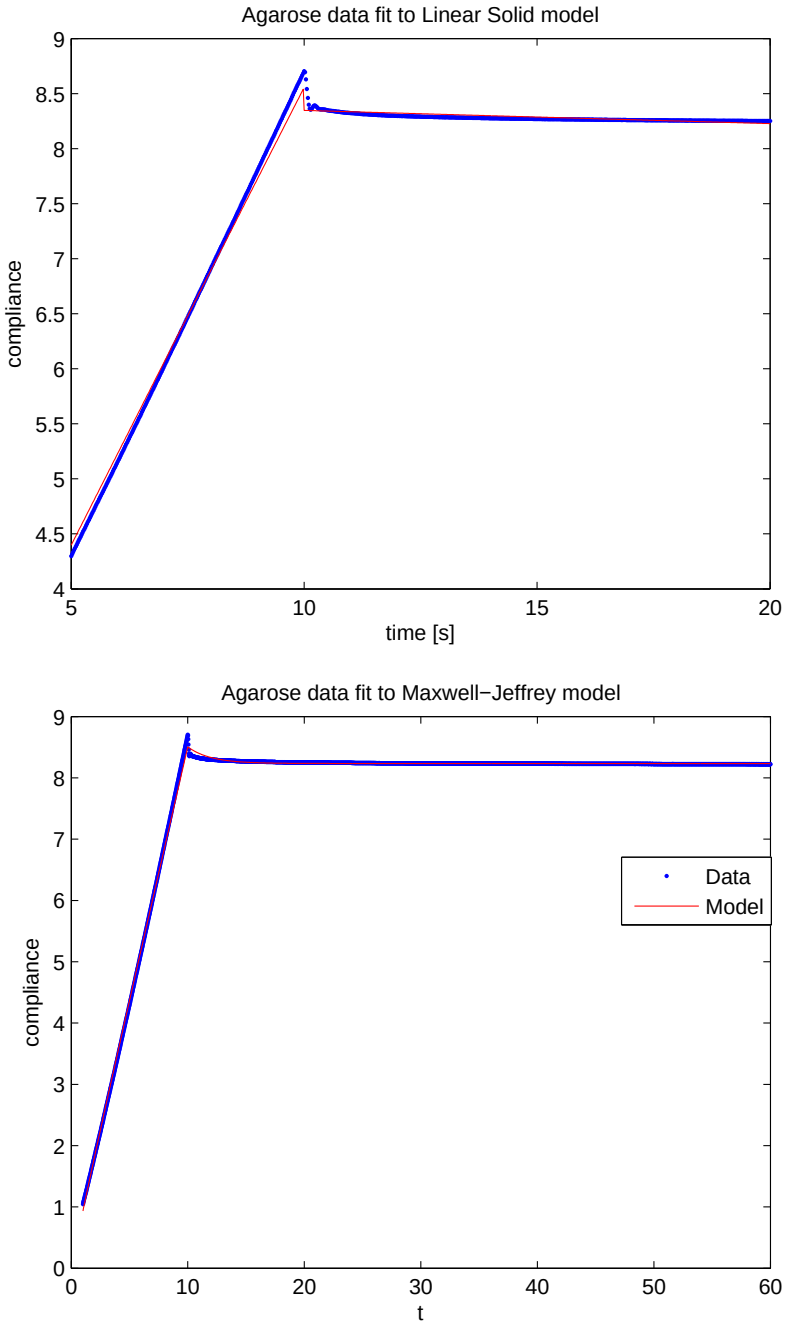

Figure 4.23: Agarose at 0.5 Pascals fit to Linear Solid and Maxwell-Jeffrey.

To illustrate how well the software can recover the parameters of exact data (data that is known not to evolve in time), we generated Inertial Maxwell-Jeffrey data with the following parameters: $G = 2, \eta_1 = 0.06, \eta_2 = 14$ and $\alpha = 0.05$. There is 1% error. The parameter_fitting_gui does not support inertial models past the force off time, so we used the interval $(0,3)$. On this interval, the frequency was calculated by fft and used as an initial guess. An initial guess of 0.1 was used for the inertial parameter α, and nothing was fixed. The program was able to recover the model with $R^2 = .9998$ on the $(0,10)$ force on region. The same results were obtained by using a large fitting interval of $(0,9)$. See Figure 4.24.

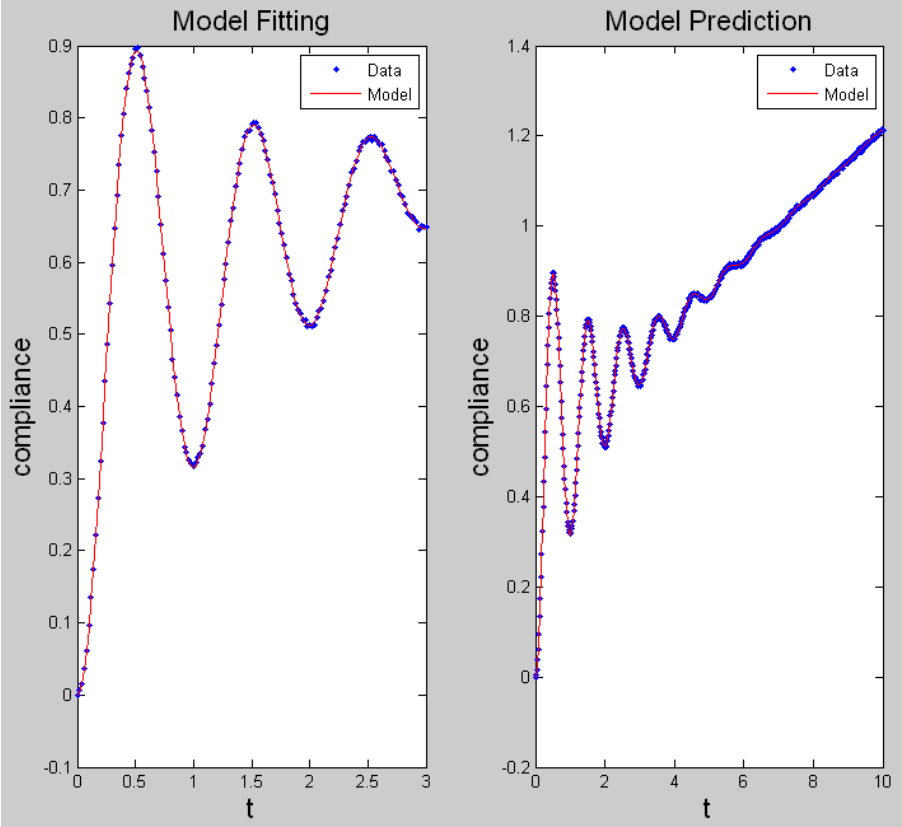

Figure 4.24: The fitting software is able to recover exact inertial data to high accuracy.

Now consider some experimental inertial data. An interval of $(0,5)$ was used to calculate the frequency and to perform the fitting. The Inertial Maxwell Jeffrey model was used because of the overall positive slope of the oscillations (not captured by Inertial Voigt). There is decent

accuracy obtained for the interval, however the remainder of the data does not fit the predicted model. See Figure 4.25. The parameters returned for the small interval were $G = 2.804$, $\eta_1 = 21.107$, $\eta_2 = 0.139$ and $\alpha = 0.047$. To attempt to find better fits to the data, we will try

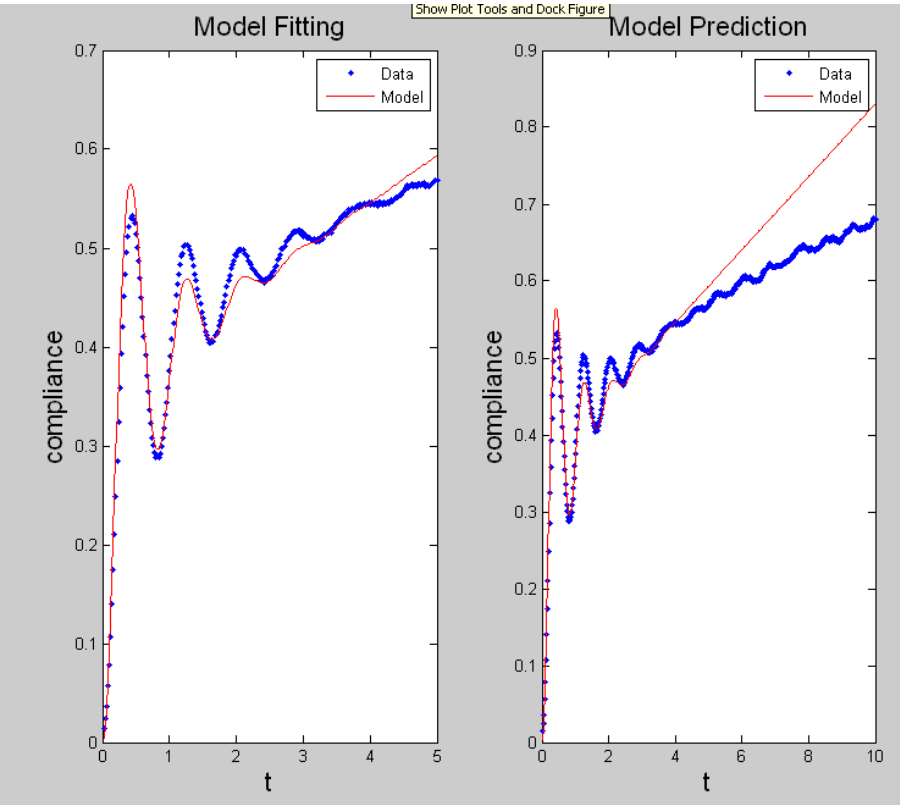

Figure 4.25: The fitting software produces a decent fit on the fitting interval (0, 5), but fails to accurately model the rest of the data.

fitting successively to smaller windows. Using 1 second intervals, we find excellent accuracy over the interval, but the model does not match the rest of the data. The parameter results for the first three intervals are given:

Interval :	G	η_1	η_2	α
$[0,1]$	3.527	6.864	0.097	0.061
$[1,2]$	2.808	17.314	0.11	0.047
$[2,3]$	2.666	22.151	0.103	0.044

Without taking any more intervals, we can see that the parameters are changing quickly during the experiment, some more than others. This certainly provides evidence that either the response of this data is nonlinear, or that thixotropy has occurred during the experiment.

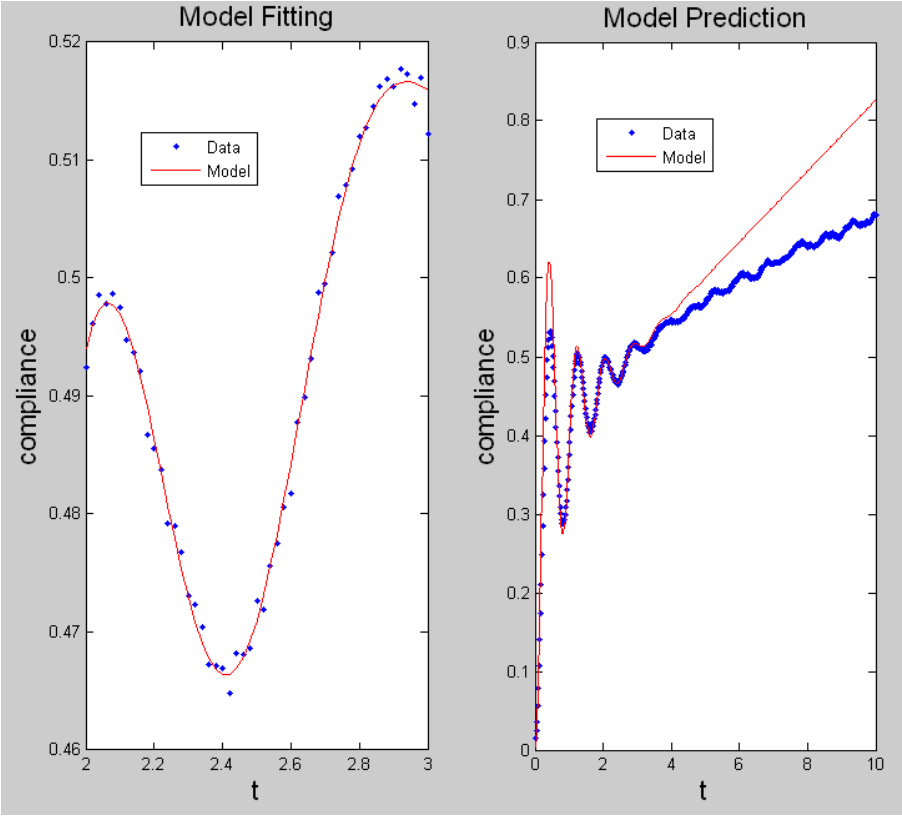

Figure 4.26: The fitting software produces a decent fit on the very small interval (2, 3), but fails to accurately model the rest of the data.

Bibliography

Baravian, C., Quemada, D., "Using Instrumental Inertia in Controlled Stress Rheometry," *Rheol Acta*, 37:223-233, Jan 1998.

Macosko, C., *Rheology: Principles, Measurements, and Applications*; Wiley-VCH: New York, 1994.

Tschoegl, N., *The Phenomenological Theory of Linear Viscoelastic Bahvior: an Introduction*; Springer: New York, 1989.

Xu, K., "Mathematics of Microrheology with Applications to Pulmonary Liquids," Ph.D. thesis, University of North Carolina at Chapel Hill, 2009.